Electronic Supplementary Information

for

DFT study on MgAl-layered double hydroxides with different interlayer anions: structure, anion exchange, host-guest interaction and basic sites

Hui-Min Liu,‡ Xiao-Jie Zhao,‡ Yu-Quan Zhu, Hong Yan*

State Key Laboratory of Chemical Resource Engineering, College of Chemistry, Beijing University of Chemical Technology, 100029, Beijing, P. R. China

Corresponding Authors

*(H. Y.) Tel: +86-010-64448331. E-mail: yanhong@mail.buct.edu.cn.

‡ These authors contributed equally to this work.

1 # Contents

2

	The electronic density difference of interlayer species of MgAl-A-LDHs interlayered with different anions (A= F^-, Cl^-, Br^-, I^-, OH^-, NO_3^-, CO_3^{2-}, SO_4^{2-}, PO_4^{3-}) and different *R* (Mg^{2+}/Al^{3+}) under the top view. The color of each element is listed.	Fig. S7
	The electronic density difference of the layer and interlayer species of MgAl-A-LDHs interlayered with different anions (A= F^-, Cl^-, Br^-, I^-, OH^-, NO_3^-, CO_3^{2-}, SO_4^{2-}, PO_4^{3-}) and different *R* (Mg^{2+}/Al^{3+}) (side view). The color of each element is listed.	Fig. S8
	Total density of states (TDOS) and partial density of states (PDOS) for the MgAl-A-LDHs intercalated with different interlayer anions (A= F^-, Cl^-, Br^-, I^-, OH^-, NO_3^-, CO_3^{2-}, SO_4^{2-}, PO_4^{3-}) and different *R* (Mg^{2+}/Al^{3+}). The Fermi energy is shown as a dashed vertical line, and has been set as 0 eV.	Fig. S9

1

2

The determination of the cut–off energy

According to the state of the art, the cut-off energy applied in the plane wave basis set ranges from 340 eV to 540 eV[S1-S3]. Increasing the value of the cut-off energy can aggrandize the accuracy of the calculation, with the augmented computational cost at the same time. In this work, the geometry of model Mg_2Al-Cl-LDHs was optimized under the cut–off energy ranging from 300 eV to 540 eV. The energy of Mg_2Al-Cl-LDHs is thus calculated to be –64540.3637 eV with the cut–off energy of 340 eV, and –64544.1677 eV with the cut-off energy of 540 eV. Therefore, the difference of the calculation results under the cut-off energy of 340 eV and 580 eV is 3.8 eV. Given that the model of Mg_2Al-Cl-LDHs contains 210 atoms, the difference under the cut-off energy of 340 eV and 580 eV is about 0.02 eV/atom. Thus, the cut–off energy of 340 eV is applied in this work.

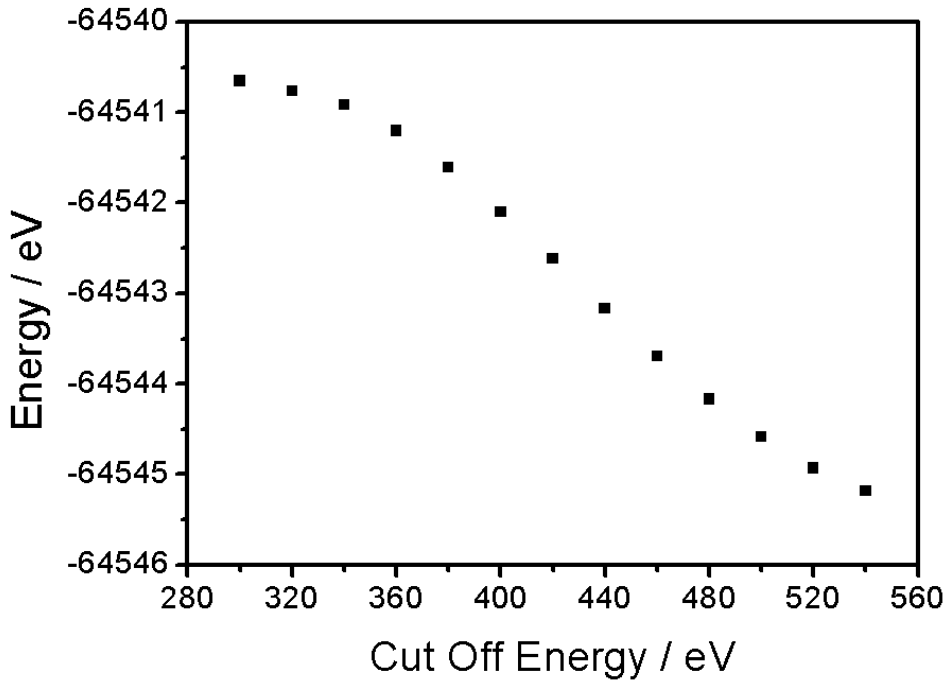

Fig. S1. The calculated energies of Mg_2Al-Cl-LDHs under the cut-off energies ranging from 300 eV to 540 eV.

The determination of computational model

The stacking sequences of the layers of LDHs include three types: three-layer rhombohedral polytype hydrotalcite (the 3R polytype), two-layer hexagonal polytype manasseite (the 2H polytype) and one-layer hexagonal polytype manasseite (the 1H polytype).[S4] For LDHs, the properties of hydroxide layers and interlayer species in different layers are similar, so we only selected LDHs in 1H and 3R configurations for verification. We optimized three models of Mg_2Al-Cl-LDHs: (1) 1H, supercell 6×6×1; (2) 3R, supercell 3×3×3; (3) 1H, supercell 6×6×3. The optimized structures are shown in Fig. S2. The lattice parameters of three optimized geometries are similar and agree well with the experimental observations, and the relative error is less than 3% (Table S3). Thus, in order to make rational use of computing resources and better research the properties of metal hydroxide layer and interlayer species, the models with 6×6×1 supercell and 1H stacking sequences are employed in this work.

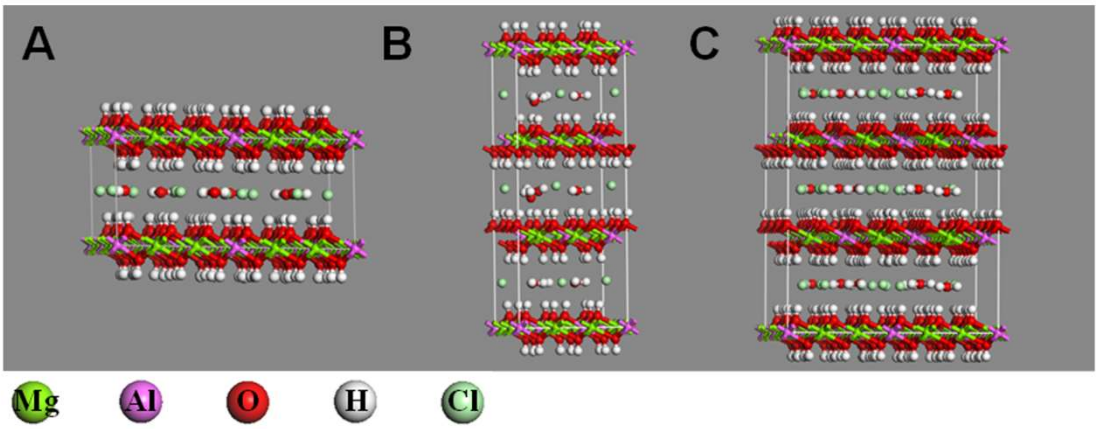

Fig. S2. The optimized structures of three model of Mg_2Al-Cl-LDHs (a) 1H, supercell 6×6×1; (b) 3R, supercell 3×3×3; (c) 1H, supercell 6×6×3.

Table S1. The experimental and calculated lattice parameters of Mg_2Al-Cl-LDHs

	Stacking sequence	Molecular formula	Supercell	Lattice parameters	
				a=*b*/Å	*c*/Å
Exptl	3R	Mg_2Al-Cl		3.08[S5-S6]	7.86[S7]
	1H	$Mg_{24}Al_{12}$-Cl_{12}	6×6×1	3.09	7.57
Calcd	3R	$Mg_{18}Al_9$-Cl_9	3×3×3	3.10	7.64
	3R	$Mg_{73}Al_{36}$-Cl_{36}	6×6×3	3.10	7.78

Table S2. The radii of different anions, the interlayer distances and total energies of MgAl-A-LDHs with different anions (F^-, Cl^-, Br^-, I^-, OH^-, NO_3^-, CO_3^{2-}, SO_4^{2-} and PO_4^{3-}) and different *R* (Mg^{2+}/Al^{3+})

A	Anion radius/ Å	*R*	Interlayer distance/Å	Total energy/ eV
F^-	1.33	1.6	7.39	–67070.4531
		2.0	7.42	–67578.6908
		2.6	7.45	–68082.7397
		3.5	7.68	–68588.6431
		5.0	7.73	–69093.4190
		8.0	7.73	–69598.7035
Cl^-	1.81	1.6	7.64	–63520.0304
		2.0	7.67	–64536.8778
		2.6	7.72	–65548.7571
		3.5	7.88	–66561.4560
		5.0	7.78	–67573.0327
		8.0	7.96	–68586.1550
Br^-	1.96	1.6	7.88	–62921.5666
		2.0	7.89	–64022.9029
		2.6	7.93	–65121.8000
		3.5	7.97	–66218.6738
		5.0	8.05	–67317.6805
		8.0	8.13	–68415.2103
I^-	2.20	1.6	8.30	–62180.0446
		2.0	8.28	–63388.2635
		2.6	8.44	–64592.6774
		3.5	8.58	–65797.2824
		5.0	8.54	–67000.2547
		8.0	8.67	–68203.2238
OH^-	1.19	1.6	7.30	–64123.5677
		2.0	7.33	–65050.7375
		2.6	6.31	–65977.4790
		3.5	7.32	–66903.2502
		5.0	7.45	–67830.3417
		8.0	7.46	–68757.0143
NO_3^-	1.65	1.6	8.79	–79868.8771
		2.0	8.94	–78549.5069
		2.6	7.88	–77225.8109
		3.5	7.78	–75904.3320
		5.0	7.86	–74580.7171
		8.0	7.92	–73257.0735
CO_3^{2-}	1.64	1.6	7.32	–68042.0411

		2.0	6.78	–68411.9841
		2.6	7.31	–68777.3695
		3.5	7.35	–69142.9019
		5.0	7.55	–69508.4645
		8.0	7.53	–69875.9562
SO_4^{2}	2.44	1.6	8.52	–71960.6140
		2.0	8.57	–71769.2235
		2.6	8.54	–71576.6295
		3.5	8.64	–71383.7383
		5.0	9.01	–71189.9591
		8.0	8.94	–70995.1161
PO_4^{3-}	2.38	1.4	8.41	–66497.1396
		2.0	8.30	–67326.7635
		3.0	8.54	–68154.2048
		5.0	8.59	–68971.7376
		8.0	8.70	–70452.6313

Table S3. The energies of ions and water

Energies of ions and water/ eV											
Mg^{2+}	Al^{3+}	OH^-	Cl^-	F^-	Br^-	I^-	NO_3^-	CO_3^{2-}	SO_4^{2-}	PO_4^{3-}	H_2O
-957.78	-35.98	-453.62	-411.67	-664.23	-369.14	-316.56	-1579.73	-1467.84	-2028.28	-1933.32	-468.72

The effect of the interlayer water molecules on the interlayer spacing of Mg_2Al-Cl-LDHs

Fig. S3 shows the interlayer spacing of Mg_2Al-Cl-LDHs containing 1, 2, 3, 4, 5, 6, 8, 10, 15, 20 numbers of water molecules. It is obvious that the interlayer spacing of LDHs increases with the increase of the number of interlayer H_2O, since more water molecules occupy more interlayer space, and the orientation of water changes from one layer to more than 2 layers. This finding also agrees well with the experimental and simulation results that the number of interlayer water molecules heavily influence the swelling property of LDHs.[50,51]

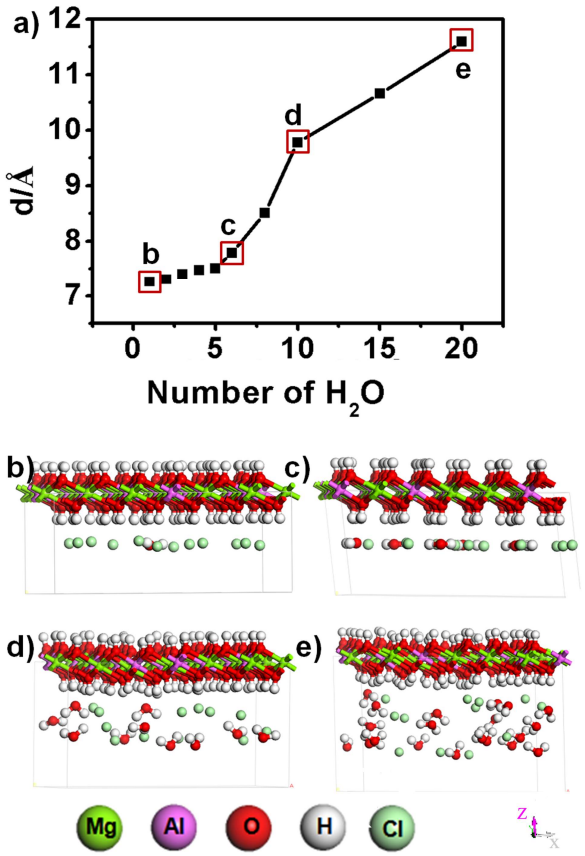

Fig. S3. The interlayer distance of Mg_2Al-Cl-LDHs intercalated with different number of interlayer water molecules.

Table S4. The interlayer distances *d* of Mg_2Al-Cl-LDHs with different number of interlayer H_2O

H_2O	1	2	3	4	5	6	8	10	15	20
d/Å	7.26	7.30	7.40	7.48	7.51	7.79	8.51	9.78	10.66	11.59

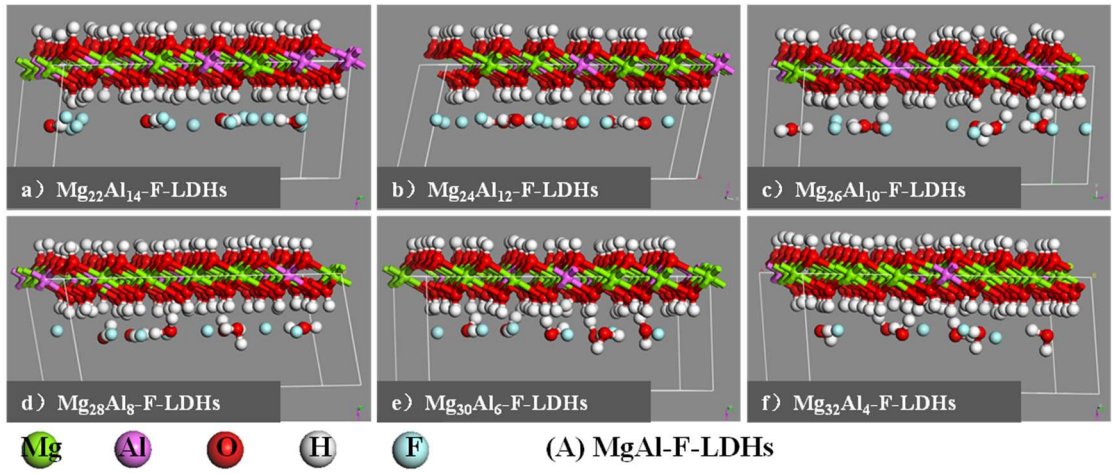

(A) MgAl-F-LDHs

1

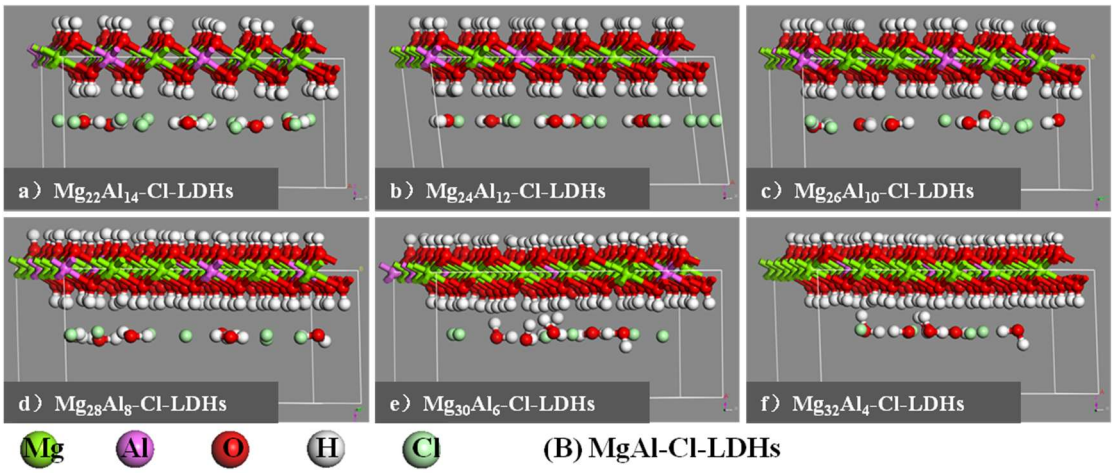

(B) MgAl-Cl-LDHs

2

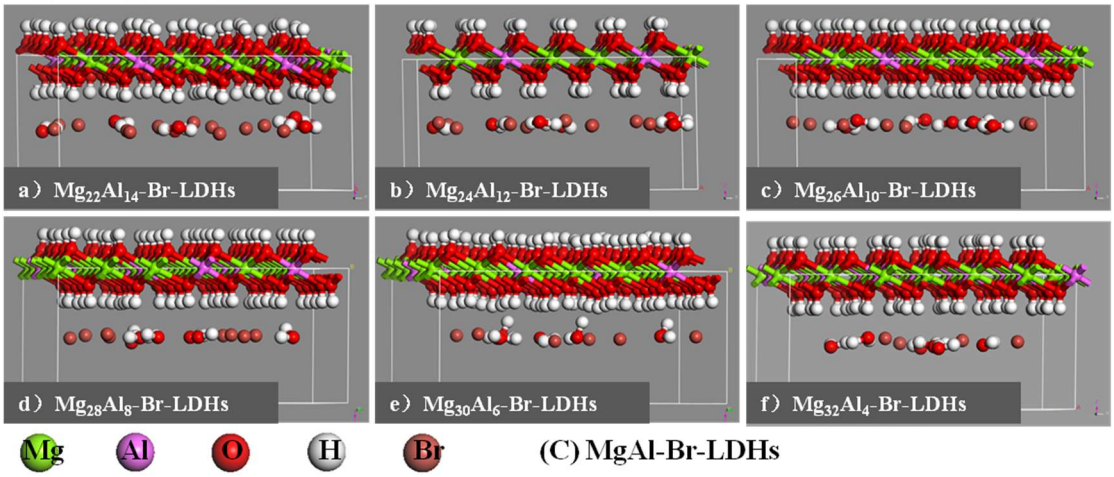

(C) MgAl-Br-LDHs

3

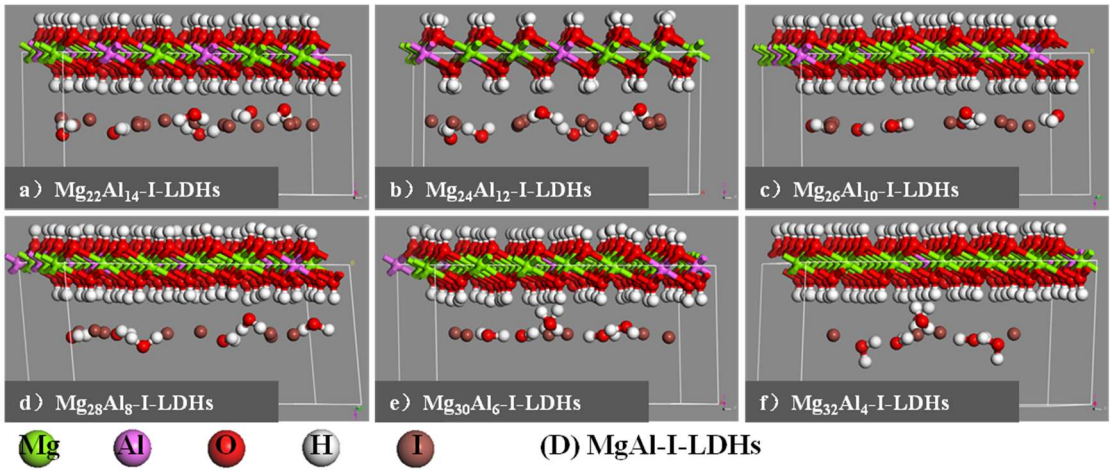

(D) MgAl-I-LDHs

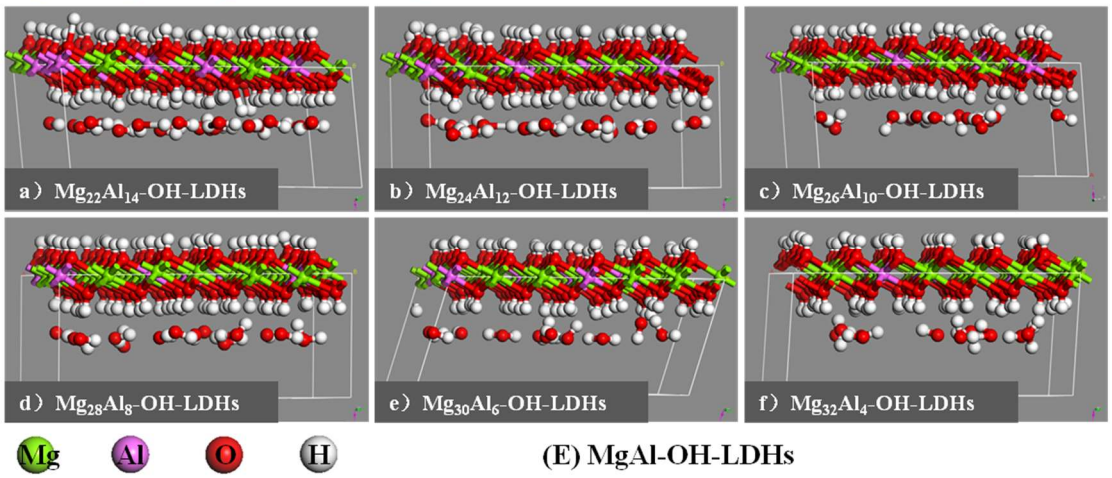

(E) MgAl-OH-LDHs

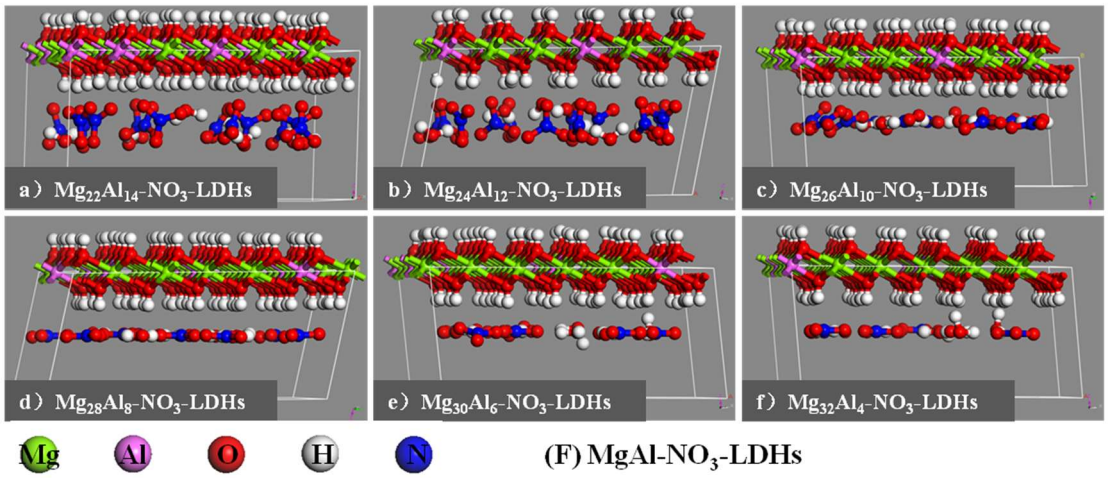

(F) MgAl-NO_3-LDHs

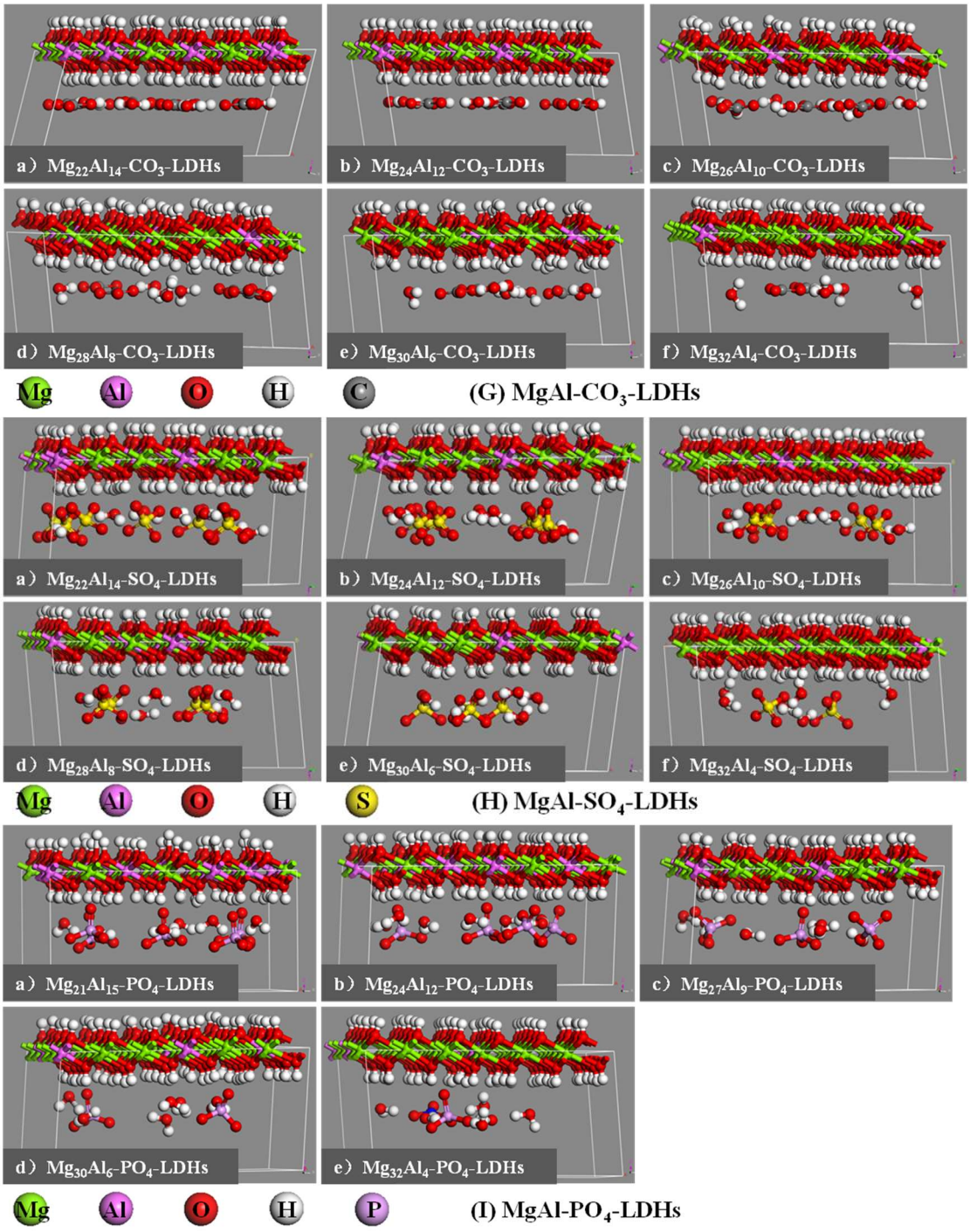

Fig. S4. The optimized structures of Mg_nAl-A-LDHs intercalated with different anions (A= F^-, Cl^-, Br^-, I^-, OH^-, NO_3^-, CO_3^{2-}, SO_4^{2-}, PO_4^{3-}), for monovalent anions and divalent anions, n=1.6, 2.0, 2.6, 3.5, 5.0 and 8.0; for trivalent anions, n= 1.4, 2.0, 3.0, 5.0 and 8.0). The color of each element is listed.

The effect of the charges of the interlayer anions on the binding energies of MgAl-LDHs

The binding energy decreases when *R* increasing. But the binding energies of the LDHs with different-charged anions at the same *R* are apparently different, changing as the following sequence: trivalent > divalent > monovalent, which indicates that the binding energy is mainly affected by the anions' charge. The higher the anion charge is, the stronger affinity between LDHs hosts and guests, leading to the easier for the anions to intercalate into the interlayer space. This is in accordance with the fact that the anions with higher charge are easier to be introduced in to the LDHs interlayer.[47, 52]

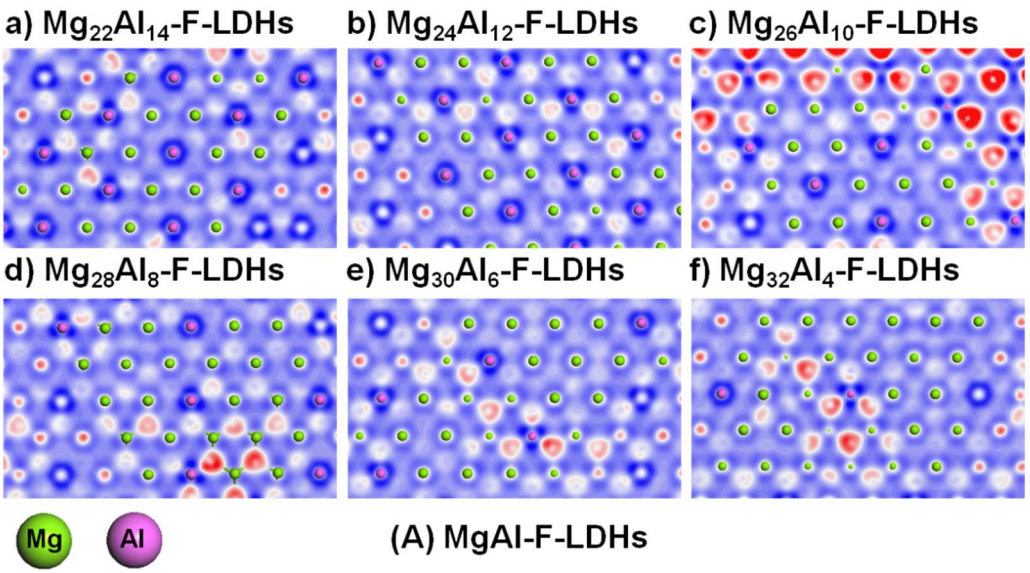
a) $Mg_{22}Al_{14}$-F-LDHs
b) $Mg_{24}Al_{12}$-F-LDHs
c) $Mg_{26}Al_{10}$-F-LDHs
d) $Mg_{28}Al_{8}$-F-LDHs
e) $Mg_{30}Al_{6}$-F-LDHs
f) $Mg_{32}Al_{4}$-F-LDHs
Mg
Al
(A) MgAl-F-LDHs

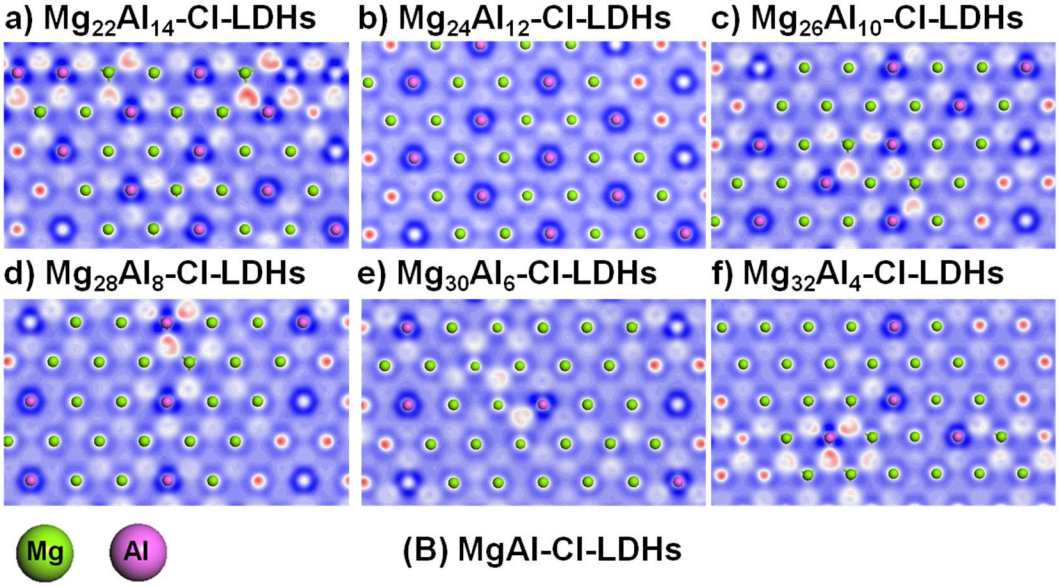
a) $Mg_{22}Al_{14}$-Cl-LDHs
b) $Mg_{24}Al_{12}$-Cl-LDHs
c) $Mg_{26}Al_{10}$-Cl-LDHs
d) $Mg_{28}Al_{8}$-Cl-LDHs
e) $Mg_{30}Al_{6}$-Cl-LDHs
f) $Mg_{32}Al_{4}$-Cl-LDHs
Mg
Al
(B) MgAl-Cl-LDHs

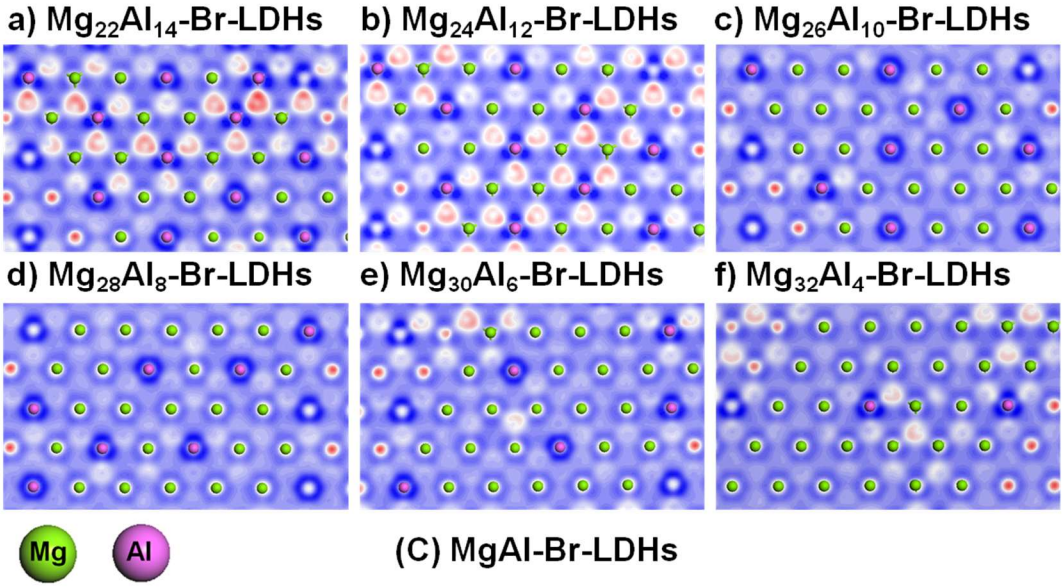
a) $Mg_{22}Al_{14}$-Br-LDHs
b) $Mg_{24}Al_{12}$-Br-LDHs
c) $Mg_{26}Al_{10}$-Br-LDHs
d) $Mg_{28}Al_{8}$-Br-LDHs
e) $Mg_{30}Al_{6}$-Br-LDHs
f) $Mg_{32}Al_{4}$-Br-LDHs
Mg
Al
(C) MgAl-Br-LDHs

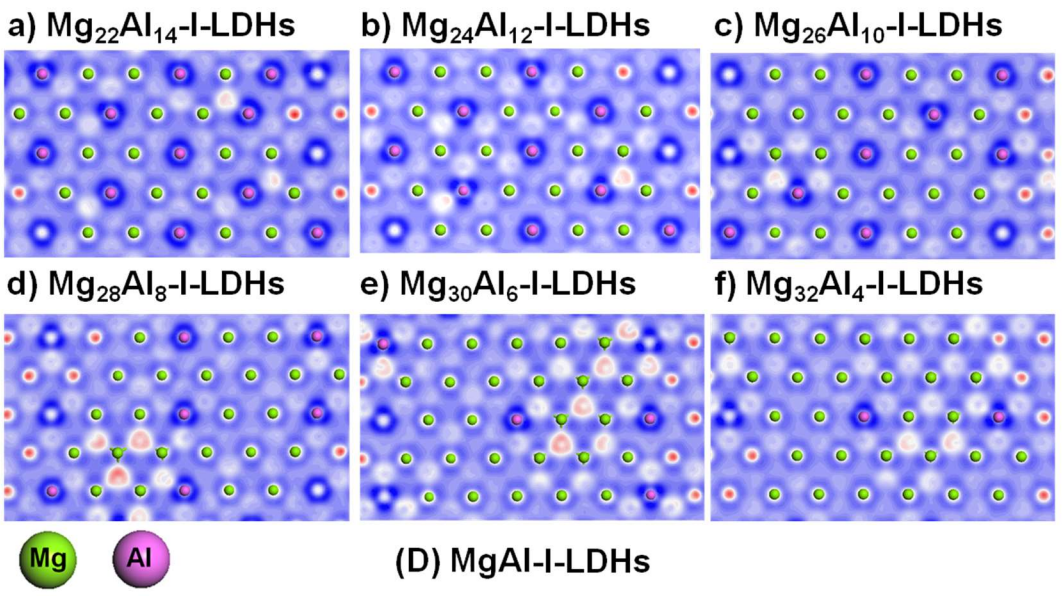
a) $Mg_{22}Al_{14}$-I-LDHs
b) $Mg_{24}Al_{12}$-I-LDHs
c) $Mg_{26}Al_{10}$-I-LDHs
d) $Mg_{28}Al_{8}$-I-LDHs
e) $Mg_{30}Al_{6}$-I-LDHs
f) $Mg_{32}Al_{4}$-I-LDHs
Mg
Al
(D) MgAl-I-LDHs

1

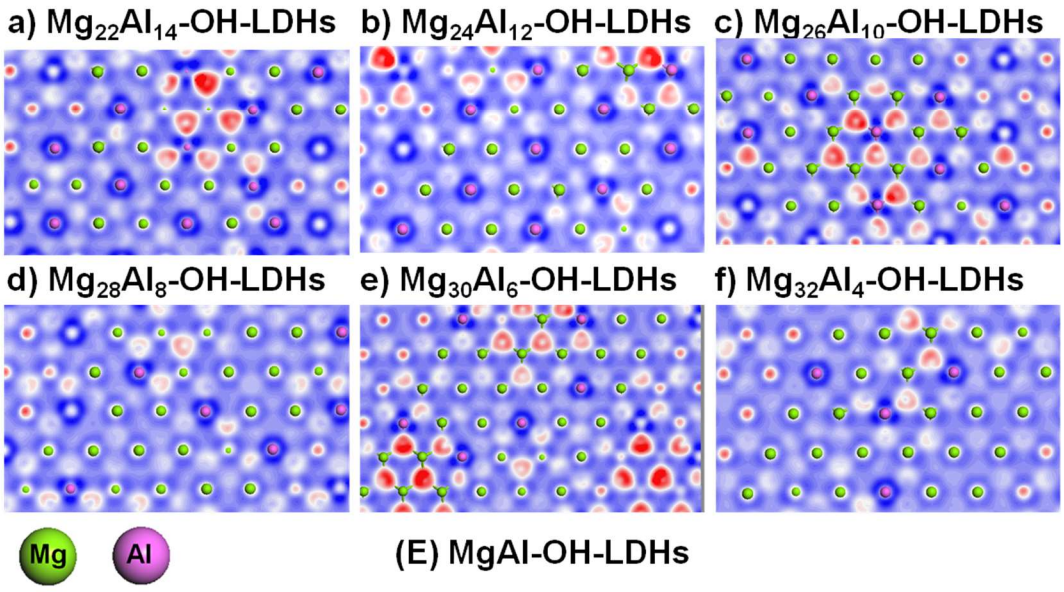
a) $Mg_{22}Al_{14}$-OH-LDHs
b) $Mg_{24}Al_{12}$-OH-LDHs
c) $Mg_{26}Al_{10}$-OH-LDHs
d) $Mg_{28}Al_{8}$-OH-LDHs
e) $Mg_{30}Al_{6}$-OH-LDHs
f) $Mg_{32}Al_{4}$-OH-LDHs
Mg
Al
(E) MgAl-OH-LDHs

2

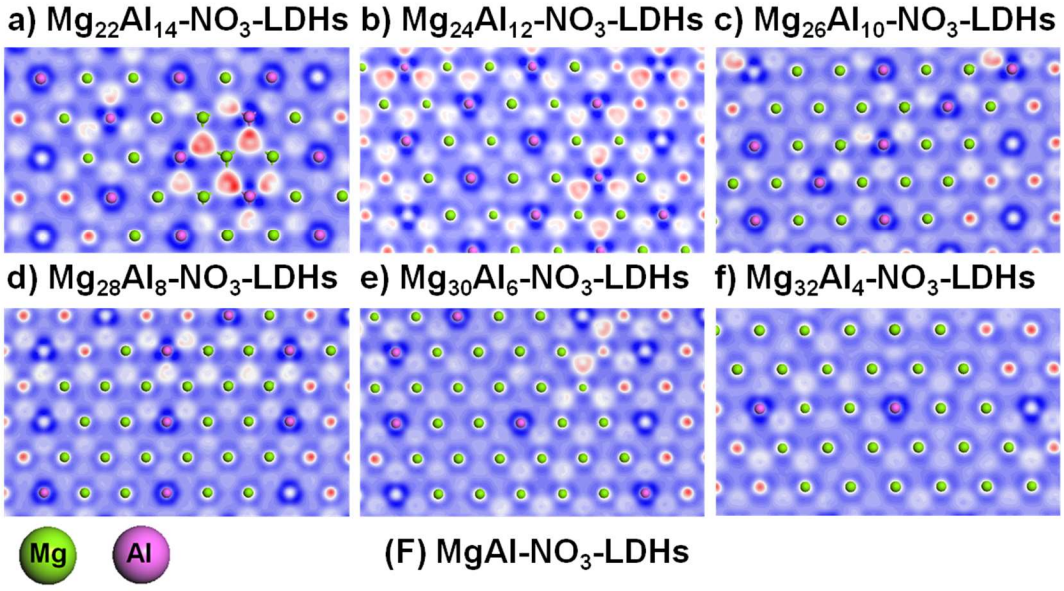
a) $Mg_{22}Al_{14}$-NO_3-LDHs
b) $Mg_{24}Al_{12}$-NO_3-LDHs
c) $Mg_{26}Al_{10}$-NO_3-LDHs
d) $Mg_{28}Al_{8}$-NO_3-LDHs
e) $Mg_{30}Al_{6}$-NO_3-LDHs
f) $Mg_{32}Al_{4}$-NO_3-LDHs
Mg
Al
(F) MgAl-NO_3-LDHs

3

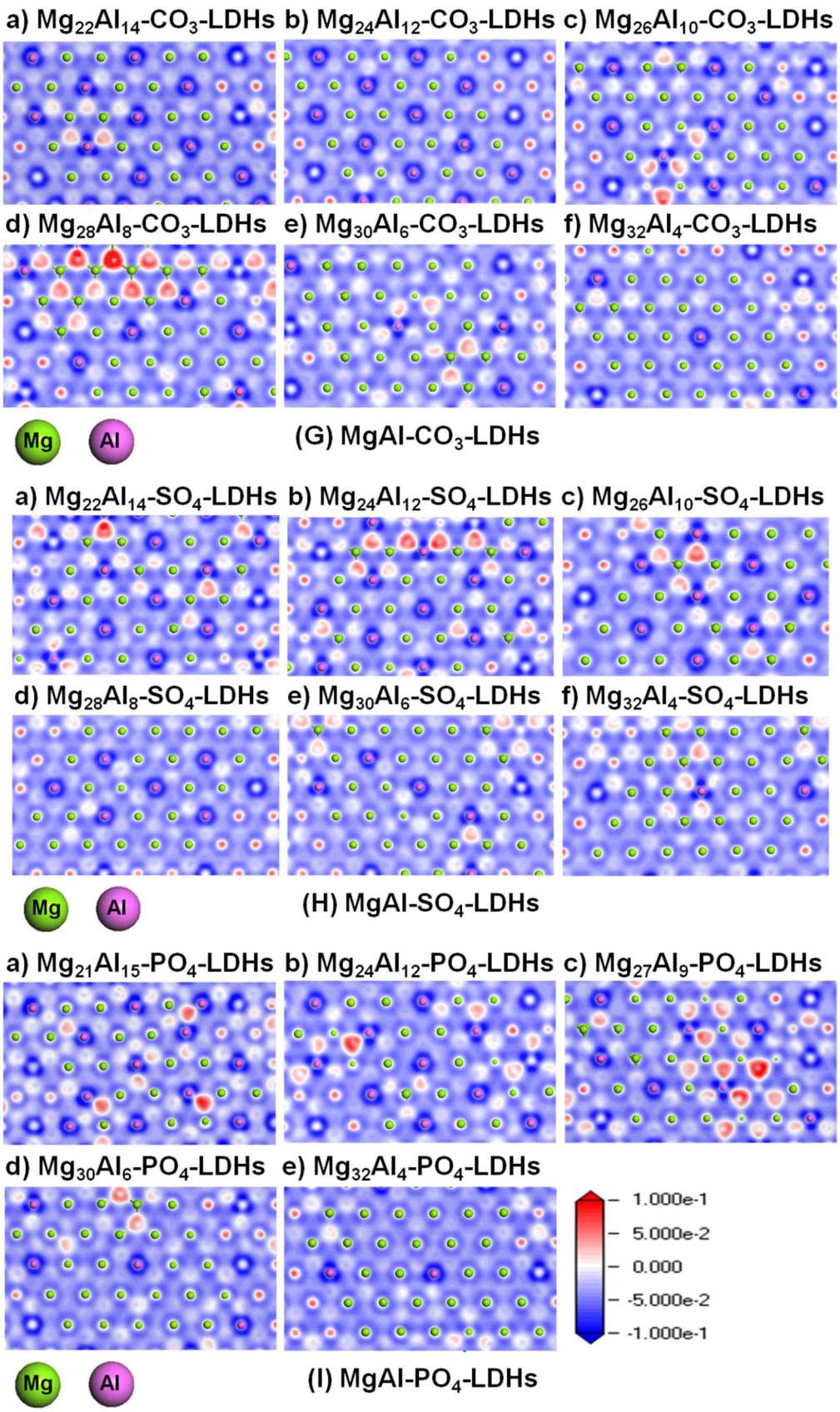

Fig. S5. The electronic density difference of layers of MgAl-A-LDHs interlayered with different anions (A= F^-, Cl^-, Br^-, I^-, OH^-, NO_3^-, CO_3^{2-}, SO_4^{2-}, PO_4^{3-}) and different R (Mg^{2+}/Al^{3+}) under the top view. The color of each element is listed.

The interaction between interlayer anions and water molecules

Fig. S6 shows the electron density difference of the interlayer species of Mg_2Al-A-LDHs with different anions with R=2 (For other R values, see Fig. S7, ESI†). As shown, there are depletion (blue) or increase (red) of electronic density around the anions and water molecules, respectively. In the case of halogen, the red color of the regions becomes more and more light in the order F^-, Cl^-, Br^-, I^-, showing that the charge accumulation of halogen is in the order $I^- < Br^- < Cl^- < F^-$. (Fig. S6a-d) This is consistent with the order of the binding energies of halogen-containing LDHs, $I^- < Br^- < Cl^- < F^-$, as mentioned in 3.3. For the remaining oxygen acid anions (NO_3^-, CO_3^{2-}, SO_4^{2-}, PO_4^{3-}, Fig. S6f–i), the red regions are around O, while the regions around N, C, S, P are in blue, demonstrating sp^n hybrid of these atoms. Furthermore, among the oxygen acid anions, CO_3^{2-} has the most significant charge accumulation with the deepest red color for O atoms (Fig. S6g), which agrees well with the fact that CO_3-LDHs are the most common LDHs in nature.[S8] It also can be seen that the blue regions around water molecules are contributed by H atom, while red is coming from O, blue and red areas overlap to display the shape of sp^3 hybrid orbital in H_2O. And the blue regions of water border on the red region of the anions (coming from halogen anions or O atoms of the oxygen acid anions and OH^-), thus the interaction between the interlayer anions and water is mainly derived from the interaction between the H atom (H') of water and halogen anions (X) or O atoms within oxygen acid anions and OH^-, where the electronic density of H of water decrease and those of the halogen anions or O within oxygen acid anions and OH^- increase. The distances of the interacted atoms ($d_{X\cdots H'}$ and $d_{O\cdots H'}$) are also displayed in Fig. S6. As shown, except for I^-, the distances are in the range from 1.5 to 2.5 Å, which can be classified to length of hydrogen bond.[56] For halogen anions, the X···H' length becomes longer in the $I^- > Br^- > Cl^- > F^-$, indicating the hydrogen bond become weaker from F to I. For the oxygen acid anions (NO_3^-, CO_3^{2-}, SO_4^{2-}, PO_4^{3-}) and OH^-, O···H shows the shortest length (strongest hydrogen bond) in CO_3^{2-}-LDH. These results

also accord to the experimental findings mentioned above. Therefore, according to the definition of hydrogen bond (IUPAC Recommendations 2011),[57] it also can be deduced that the interaction between interlayer anions and water molecules are mainly coming from the electrostatic attraction.

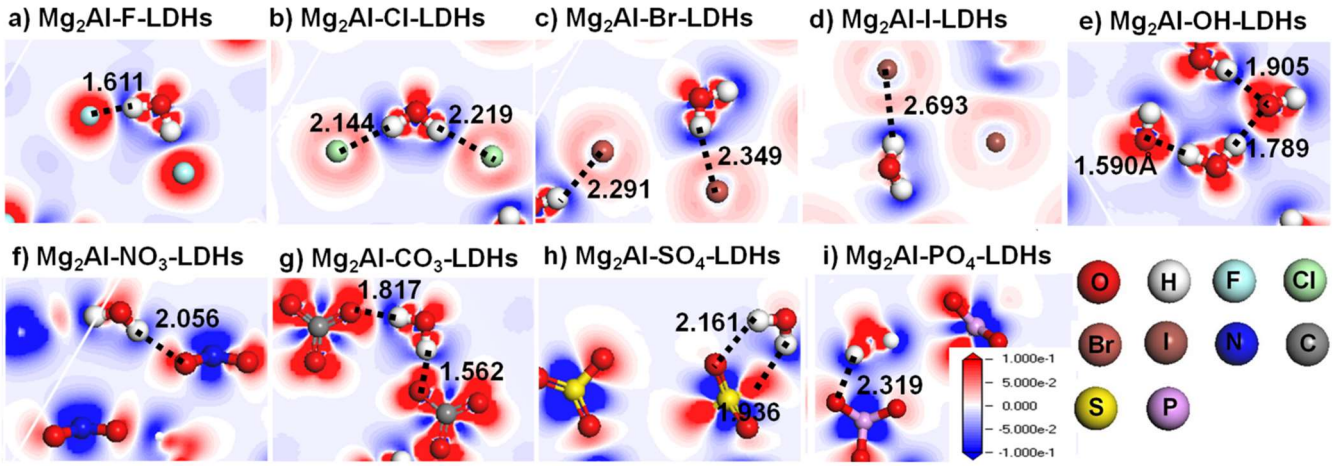

Fig. S6. The electronic density difference of interlayer species of Mg_2Al-A-LDHs interlayered with different anions (A= F^-, Cl^-, Br^-, I^-, OH^-, NO_3^-, CO_3^{2-}, SO_4^{2-} and PO_4^{3-}) under the top view, along with the distances between the H atom (H) of water and halogen anions (X) ($d_{X\ H'}$) or O atoms within oxygen acid anions ($d_{O\ H'}$) (in Å).

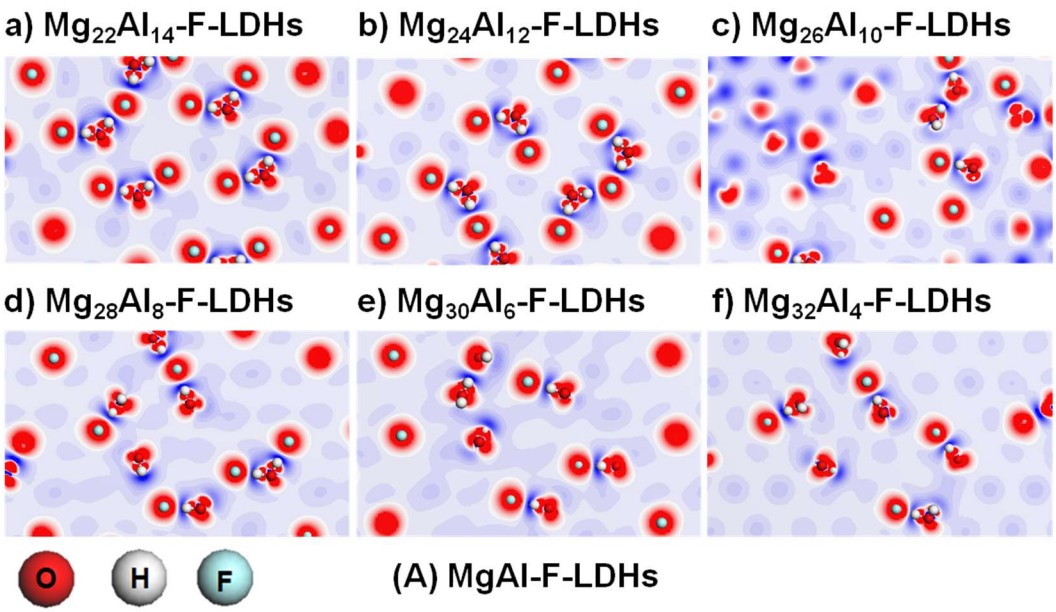
a) $Mg_{22}Al_{14}$-F-LDHs
b) $Mg_{24}Al_{12}$-F-LDHs
c) $Mg_{26}Al_{10}$-F-LDHs
d) $Mg_{28}Al_8$-F-LDHs
e) $Mg_{30}Al_6$-F-LDHs
f) $Mg_{32}Al_4$-F-LDHs
O
H
F
(A) MgAl-F-LDHs

10

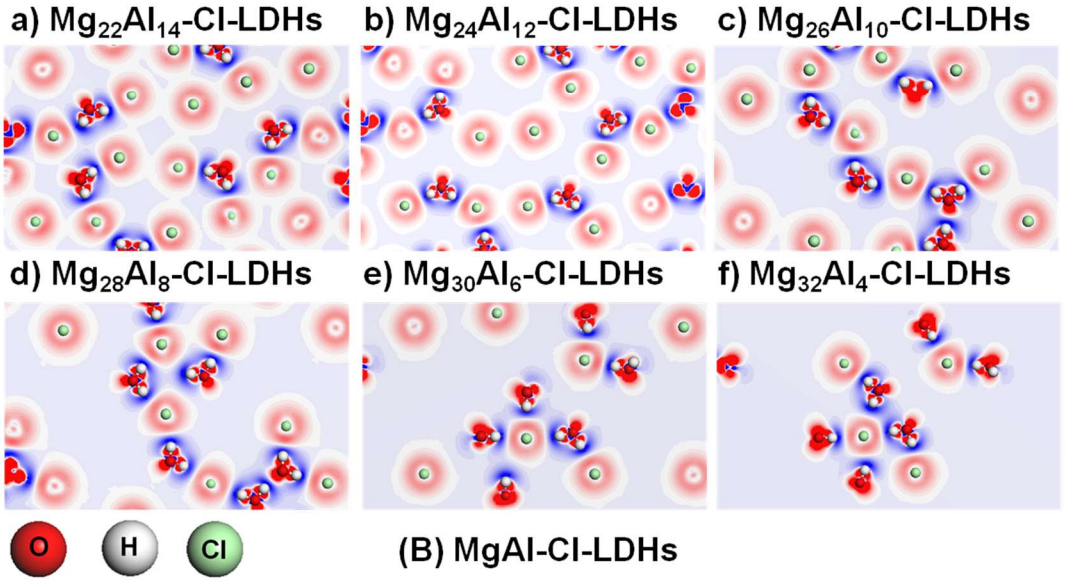
a) $Mg_{22}Al_{14}$-Cl-LDHs
b) $Mg_{24}Al_{12}$-Cl-LDHs
c) $Mg_{26}Al_{10}$-Cl-LDHs
d) $Mg_{28}Al_8$-Cl-LDHs
e) $Mg_{30}Al_6$-Cl-LDHs
f) $Mg_{32}Al_4$-Cl-LDHs
O
H
Cl
(B) MgAl-Cl-LDHs

11

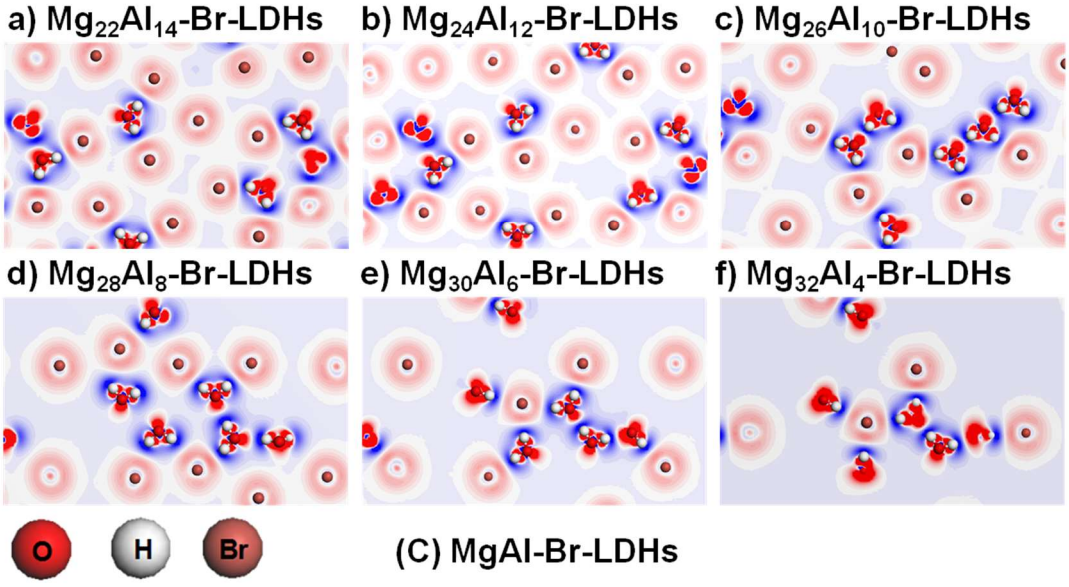
a) $Mg_{22}Al_{14}$-Br-LDHs
b) $Mg_{24}Al_{12}$-Br-LDHs
c) $Mg_{26}Al_{10}$-Br-LDHs
d) $Mg_{28}Al_8$-Br-LDHs
e) $Mg_{30}Al_6$-Br-LDHs
f) $Mg_{32}Al_4$-Br-LDHs
O
H
Br
(C) MgAl-Br-LDHs

12

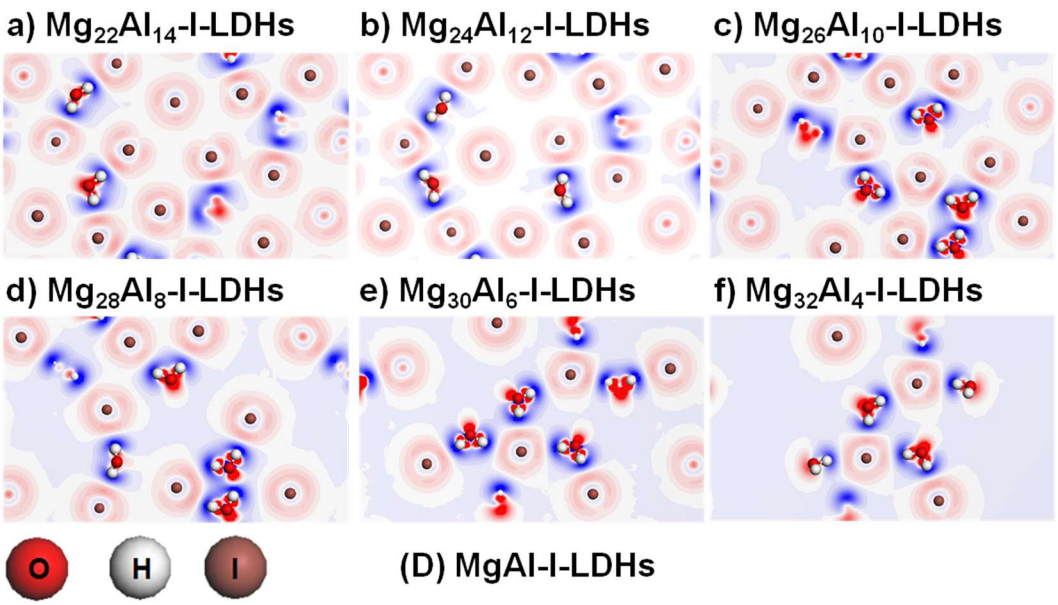
a) $Mg_{22}Al_{14}$-I-LDHs
b) $Mg_{24}Al_{12}$-I-LDHs
c) $Mg_{26}Al_{10}$-I-LDHs
d) $Mg_{28}Al_{8}$-I-LDHs
e) $Mg_{30}Al_{6}$-I-LDHs
f) $Mg_{32}Al_{4}$-I-LDHs
O
H
I
(D) MgAl-I-LDHs

13

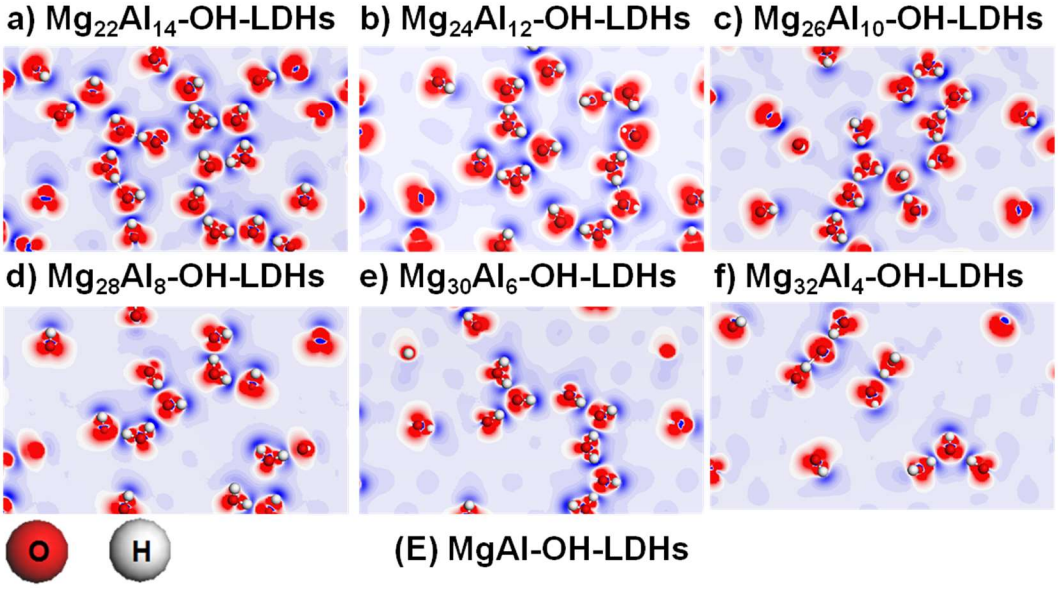
a) $Mg_{22}Al_{14}$-OH-LDHs
b) $Mg_{24}Al_{12}$-OH-LDHs
c) $Mg_{26}Al_{10}$-OH-LDHs
d) $Mg_{28}Al_{8}$-OH-LDHs
e) $Mg_{30}Al_{6}$-OH-LDHs
f) $Mg_{32}Al_{4}$-OH-LDHs
O
H
(E) MgAl-OH-LDHs

14

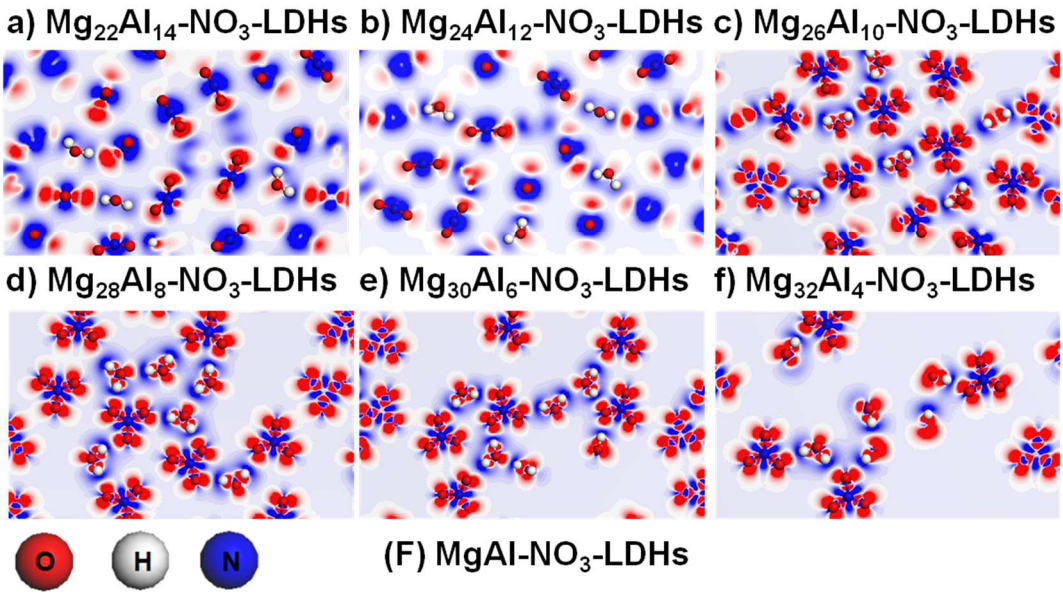
a) $Mg_{22}Al_{14}$-NO_3-LDHs
b) $Mg_{24}Al_{12}$-NO_3-LDHs
c) $Mg_{26}Al_{10}$-NO_3-LDHs
d) $Mg_{28}Al_{8}$-NO_3-LDHs
e) $Mg_{30}Al_{6}$-NO_3-LDHs
f) $Mg_{32}Al_{4}$-NO_3-LDHs
O
H
N
(F) MgAl-NO_3-LDHs

15

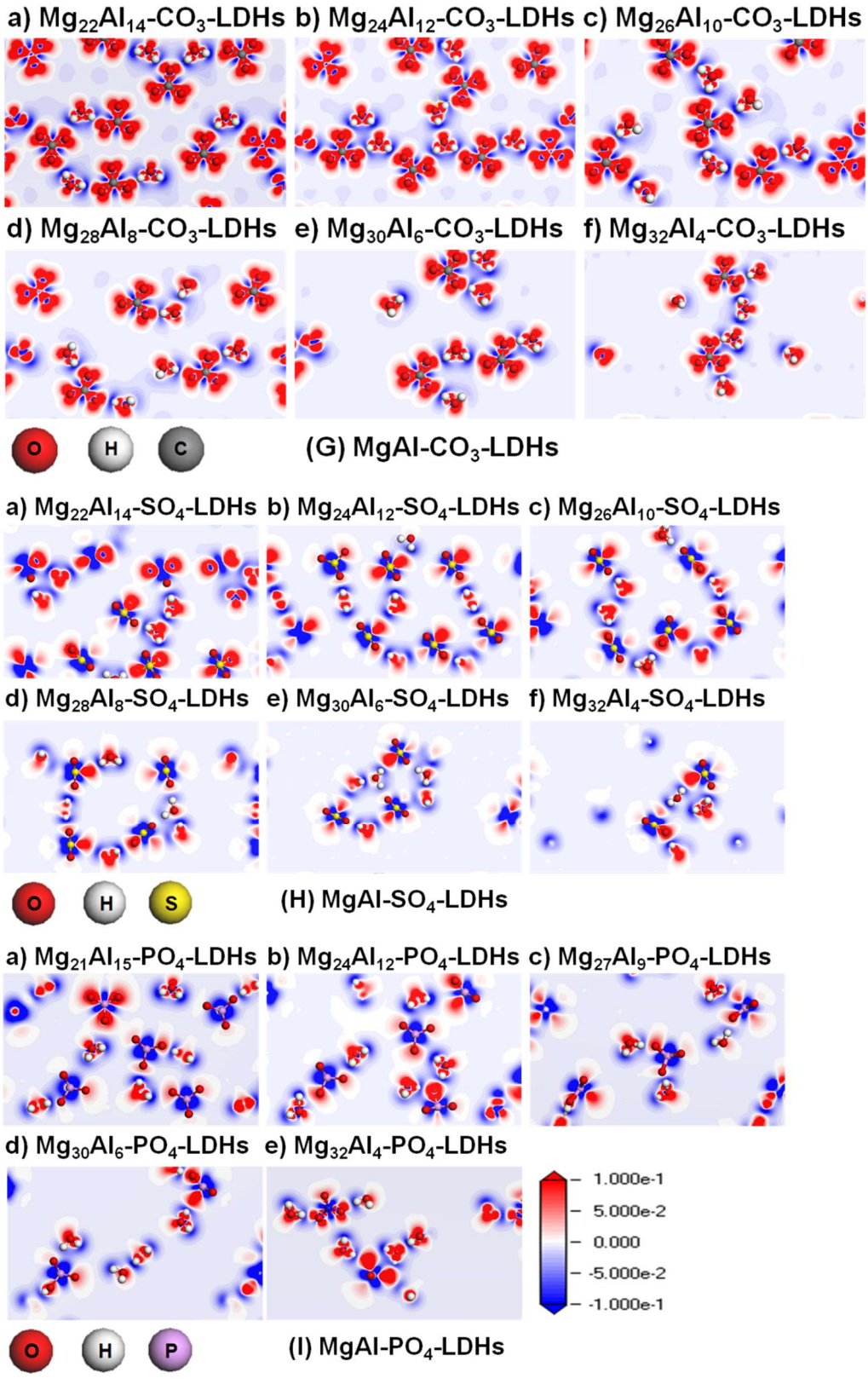

Fig. S7. The electronic density difference of interlayer species of MgAl-A-LDHs interlayered with different anions (A= F^-, Cl^-, Br^-, I^-, OH^-, NO_3^-, CO_3^{2-}, SO_4^{2-}, PO_4^{3-}) and different *R* (Mg^{2+}/Al^{3+}) under the top view. The color of each element is listed.

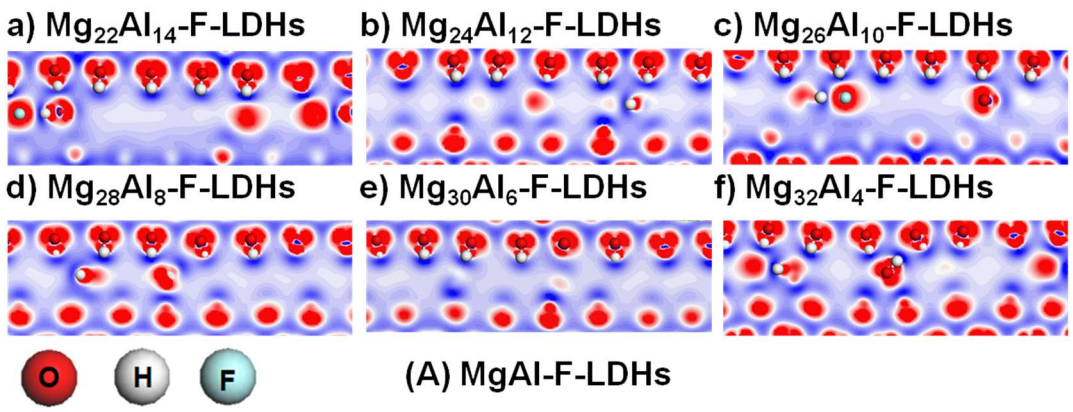
a) $Mg_{22}Al_{14}$-F-LDHs
b) $Mg_{24}Al_{12}$-F-LDHs
c) $Mg_{26}Al_{10}$-F-LDHs
d) $Mg_{28}Al_{8}$-F-LDHs
e) $Mg_{30}Al_{6}$-F-LDHs
f) $Mg_{32}Al_{4}$-F-LDHs
O
H
F
(A) MgAl-F-LDHs

22

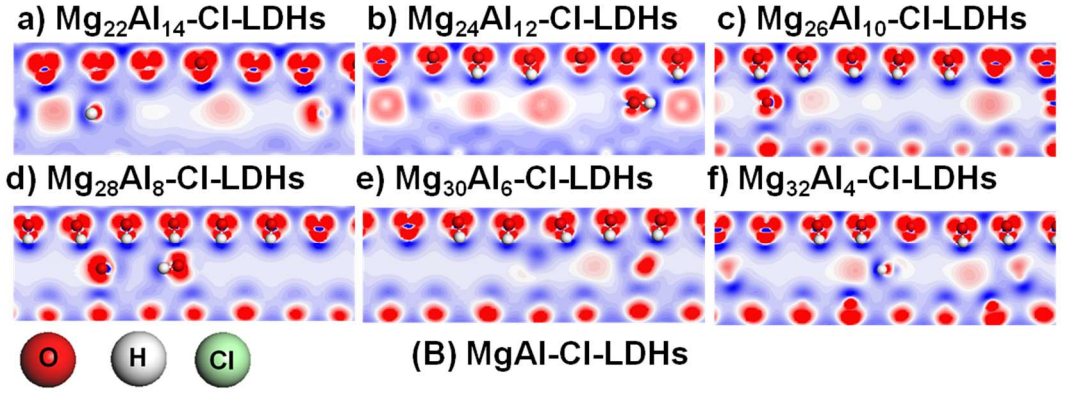
a) $Mg_{22}Al_{14}$-Cl-LDHs
b) $Mg_{24}Al_{12}$-Cl-LDHs
c) $Mg_{26}Al_{10}$-Cl-LDHs
d) $Mg_{28}Al_{8}$-Cl-LDHs
e) $Mg_{30}Al_{6}$-Cl-LDHs
f) $Mg_{32}Al_{4}$-Cl-LDHs
O
H
Cl
(B) MgAl-Cl-LDHs

23

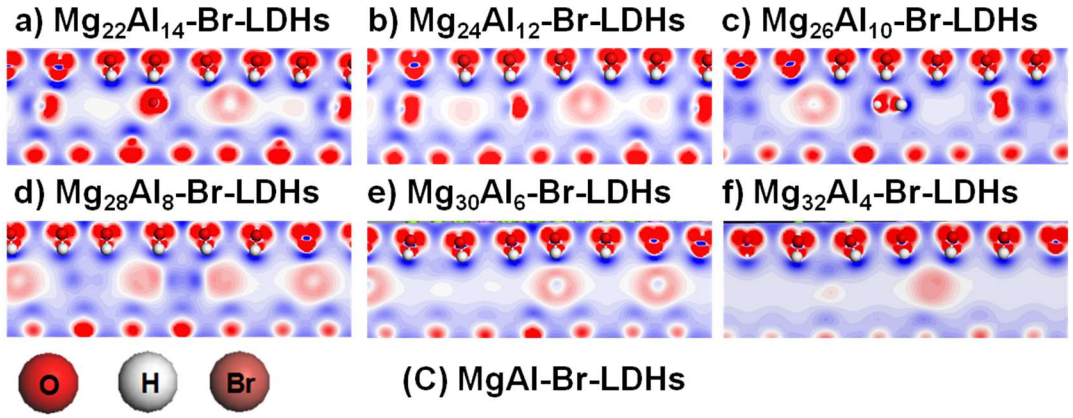
a) $Mg_{22}Al_{14}$-Br-LDHs
b) $Mg_{24}Al_{12}$-Br-LDHs
c) $Mg_{26}Al_{10}$-Br-LDHs
d) $Mg_{28}Al_{8}$-Br-LDHs
e) $Mg_{30}Al_{6}$-Br-LDHs
f) $Mg_{32}Al_{4}$-Br-LDHs
O
H
Br
(C) MgAl-Br-LDHs

24

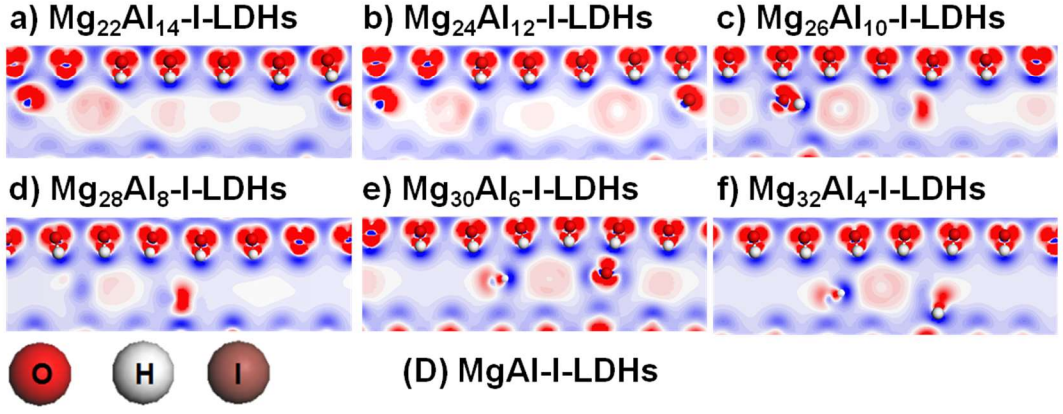
a) $Mg_{22}Al_{14}$-I-LDHs
b) $Mg_{24}Al_{12}$-I-LDHs
c) $Mg_{26}Al_{10}$-I-LDHs
d) $Mg_{28}Al_{8}$-I-LDHs
e) $Mg_{30}Al_{6}$-I-LDHs
f) $Mg_{32}Al_{4}$-I-LDHs
O
H
I
(D) MgAl-I-LDHs

25

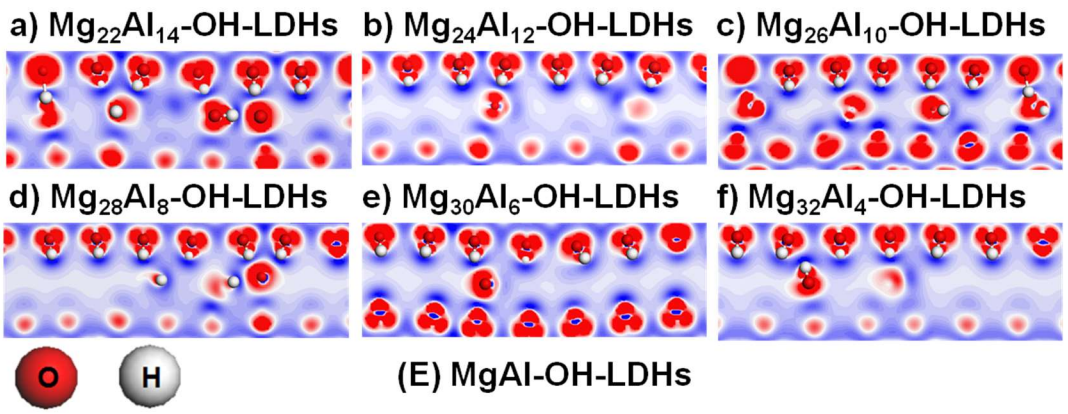
a) $Mg_{22}Al_{14}$-OH-LDHs
b) $Mg_{24}Al_{12}$-OH-LDHs
c) $Mg_{26}Al_{10}$-OH-LDHs
d) $Mg_{28}Al_{8}$-OH-LDHs
e) $Mg_{30}Al_{6}$-OH-LDHs
f) $Mg_{32}Al_{4}$-OH-LDHs
O
H
(E) MgAl-OH-LDHs

26

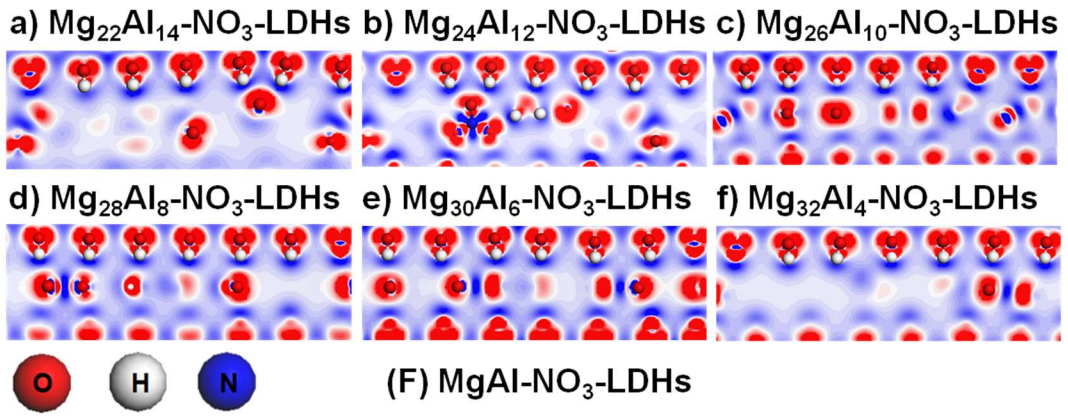
a) $Mg_{22}Al_{14}$-NO_3-LDHs
b) $Mg_{24}Al_{12}$-NO_3-LDHs
c) $Mg_{26}Al_{10}$-NO_3-LDHs
d) $Mg_{28}Al_{8}$-NO_3-LDHs
e) $Mg_{30}Al_{6}$-NO_3-LDHs
f) $Mg_{32}Al_{4}$-NO_3-LDHs
O
H
N
(F) MgAl-NO_3-LDHs

27

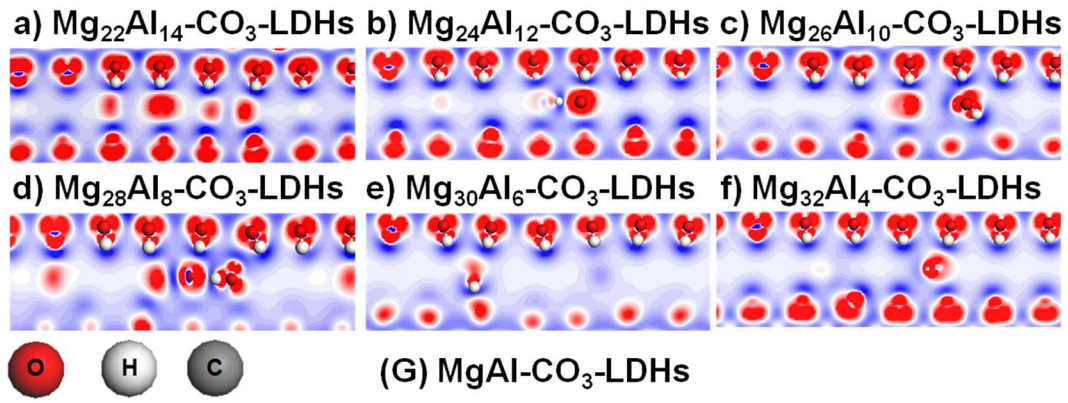
a) $Mg_{22}Al_{14}$-CO_3-LDHs
b) $Mg_{24}Al_{12}$-CO_3-LDHs
c) $Mg_{26}Al_{10}$-CO_3-LDHs
d) $Mg_{28}Al_{8}$-CO_3-LDHs
e) $Mg_{30}Al_{6}$-CO_3-LDHs
f) $Mg_{32}Al_{4}$-CO_3-LDHs
O
H
C
(G) MgAl-CO_3-LDHs

28

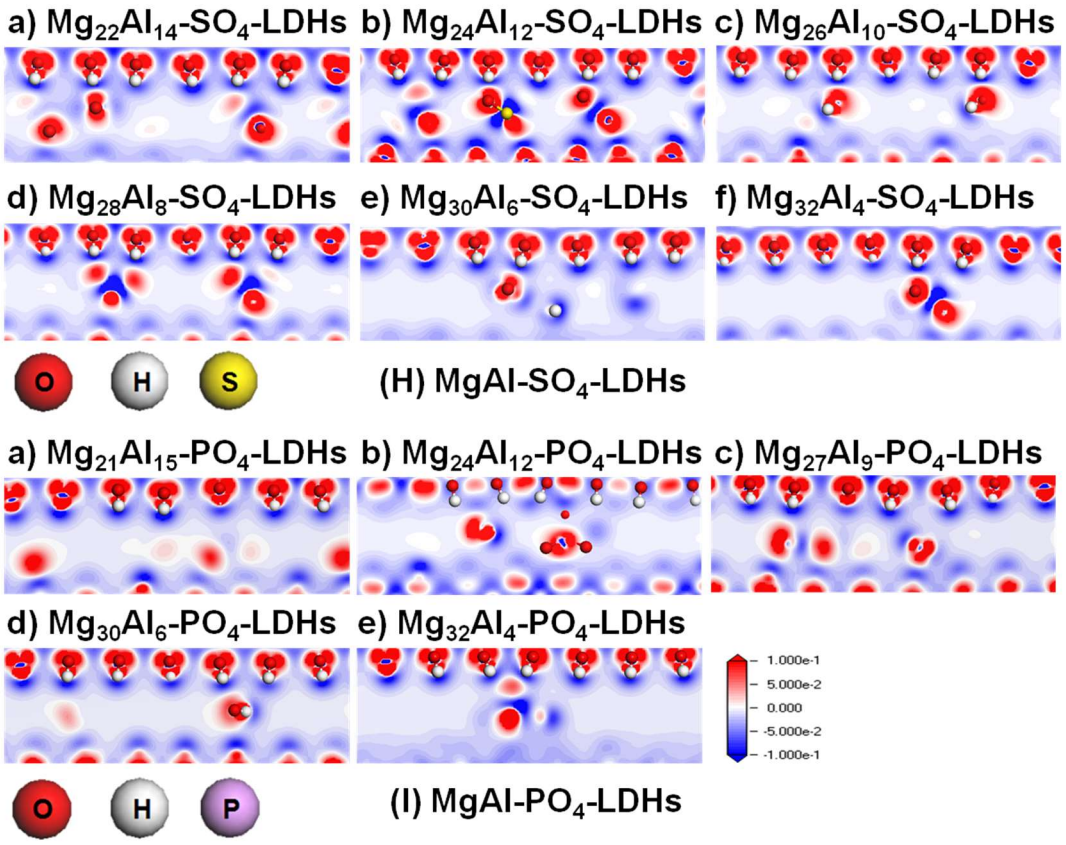

Fig. S8. The electronic density difference of the layer and interlayer species of MgAl-A-LDHs interlayered with different anions (A= F^-, Cl^-, Br^-, I^-, OH^-, NO_3^-, CO_3^{2-}, SO_4^{2-}, PO_4^{3-}) and different *R* (Mg^{2+}/Al^{3+}) (side view). The color of each element is listed.

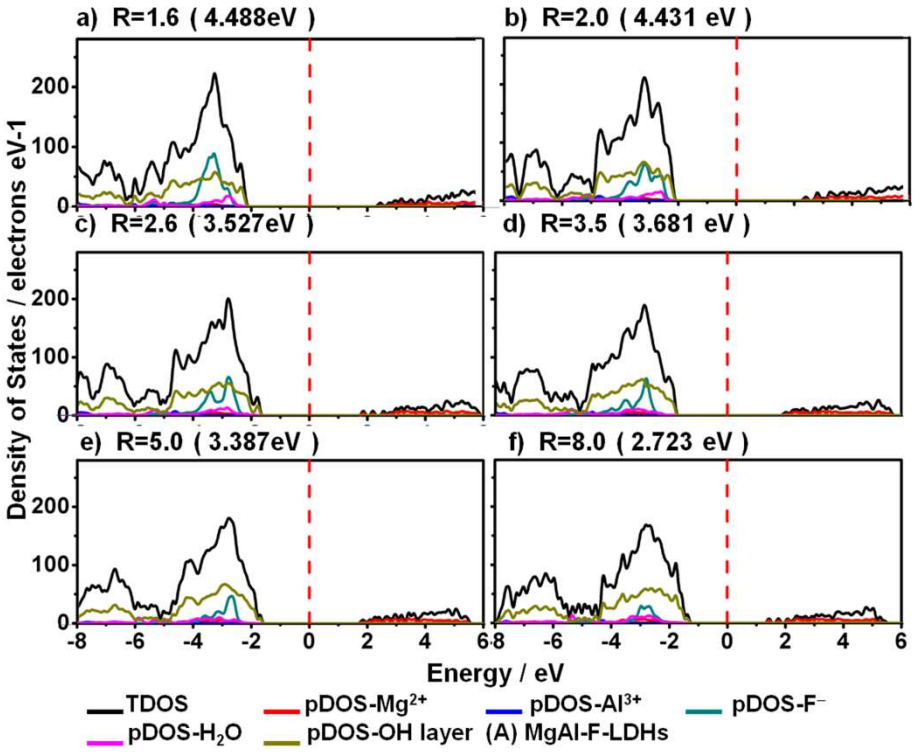
a) R=1.6 (4.488eV)
b) R=2.0 (4.431 eV)
c) R=2.6 (3.527eV)
d) R=3.5 (3.681 eV)
e) R=5.0 (3.387eV)
f) R=8.0 (2.723 eV)
Density of States / electrons eV-1
Energy / eV
TDOS
pDOS-Mg2+
pDOS-Al3+
pDOS-F−
pDOS-H2O
pDOS-OH layer
(A) MgAl-F-LDHs

34

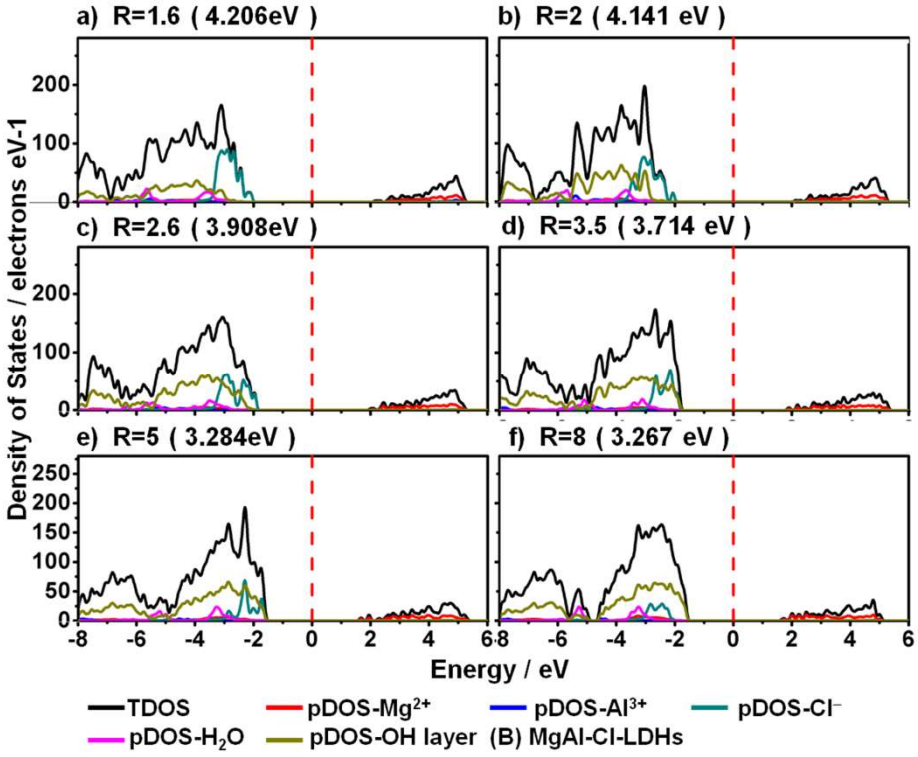
a) R=1.6 (4.206eV)
b) R=2 (4.141 eV)
c) R=2.6 (3.908eV)
d) R=3.5 (3.714 eV)
e) R=5 (3.284eV)
f) R=8 (3.267 eV)
Density of States / electrons eV-1
Energy / eV
TDOS
pDOS-Mg2+
pDOS-Al3+
pDOS-Cl−
pDOS-H2O
pDOS-OH layer
(B) MgAl-Cl-LDHs

35

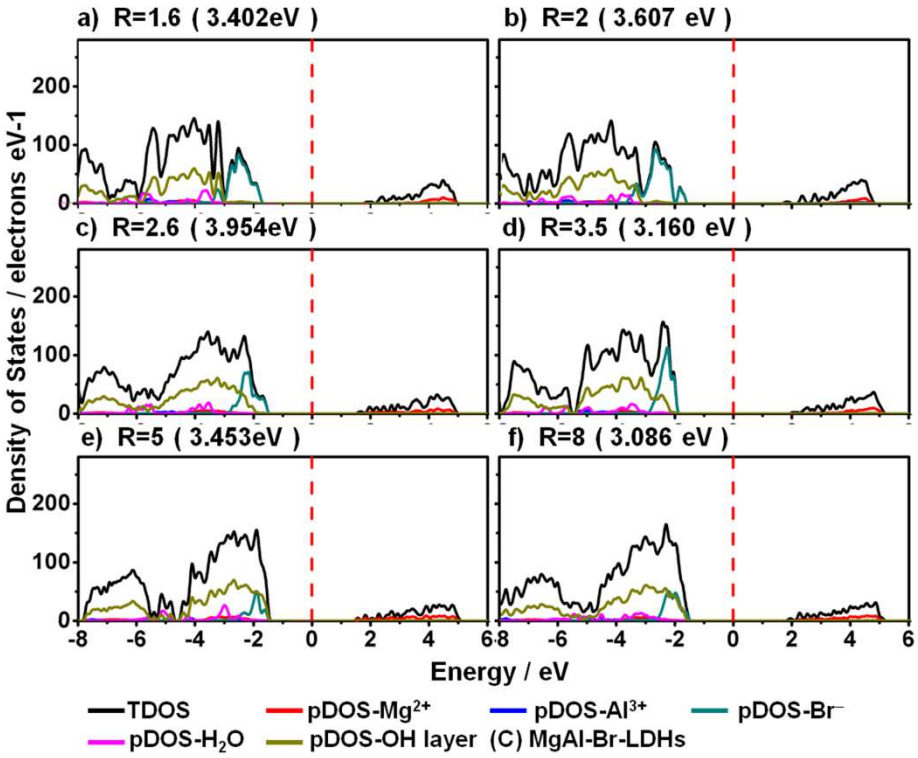
a) R=1.6 (3.402eV)
b) R=2 (3.607 eV)
c) R=2.6 (3.954eV)
d) R=3.5 (3.160 eV)
e) R=5 (3.453eV)
f) R=8 (3.086 eV)
Density of States / electrons eV-1
Energy / eV
TDOS
pDOS-Mg2+
pDOS-Al3+
pDOS-Br−
pDOS-H2O
pDOS-OH layer
(C) MgAl-Br-LDHs

36

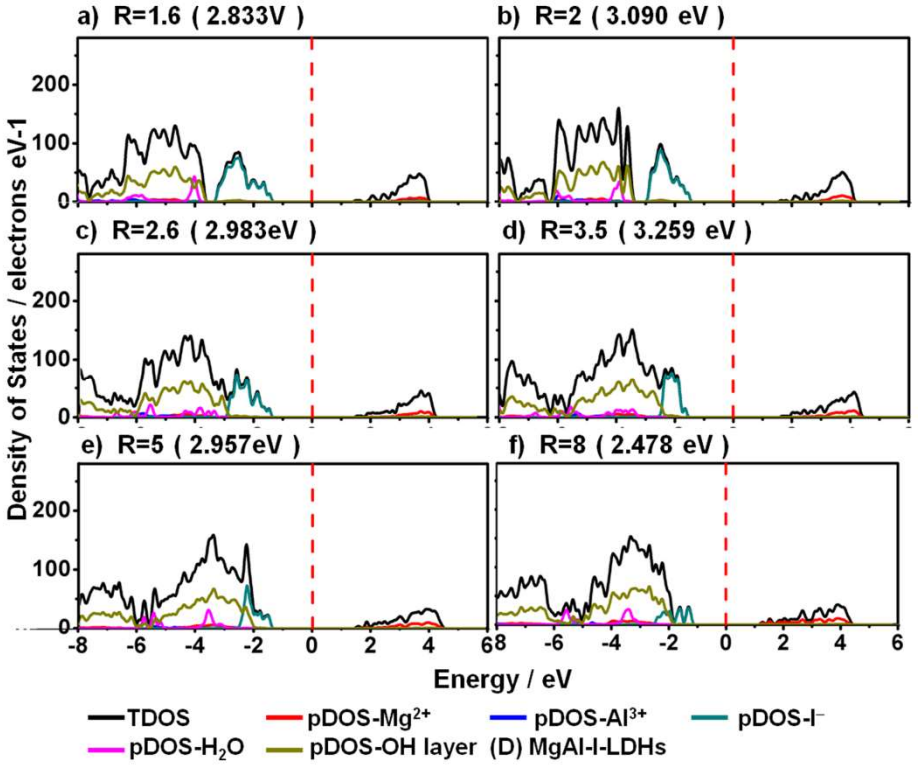
a) R=1.6 (2.833V)
b) R=2 (3.090 eV)
c) R=2.6 (2.983eV)
d) R=3.5 (3.259 eV)
e) R=5 (2.957eV)
f) R=8 (2.478 eV)
Density of States / electrons eV-1
Energy / eV
TDOS
pDOS-Mg2+
pDOS-Al3+
pDOS-I−
pDOS-H2O
pDOS-OH layer
(D) MgAl-I-LDHs

37

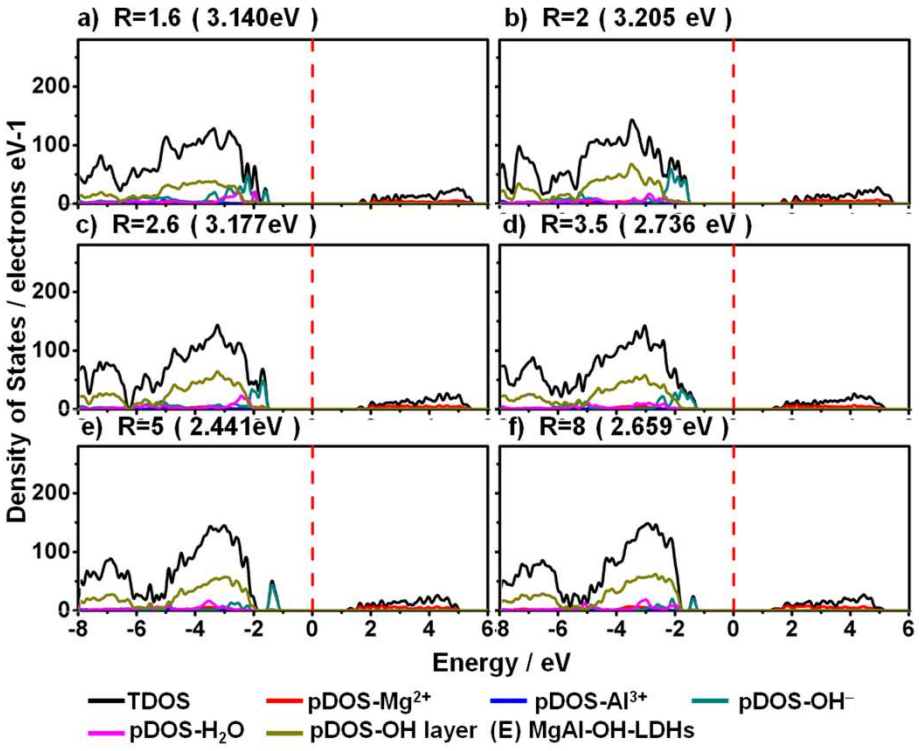
a) R=1.6 (3.140eV)
b) R=2 (3.205 eV)
c) R=2.6 (3.177eV)
d) R=3.5 (2.736 eV)
e) R=5 (2.441eV)
f) R=8 (2.659 eV)
Density of States / electrons eV-1
Energy / eV
TDOS
pDOS-Mg2+
pDOS-Al3+
pDOS-OH−
pDOS-H2O
pDOS-OH layer
(E) MgAl-OH-LDHs

38

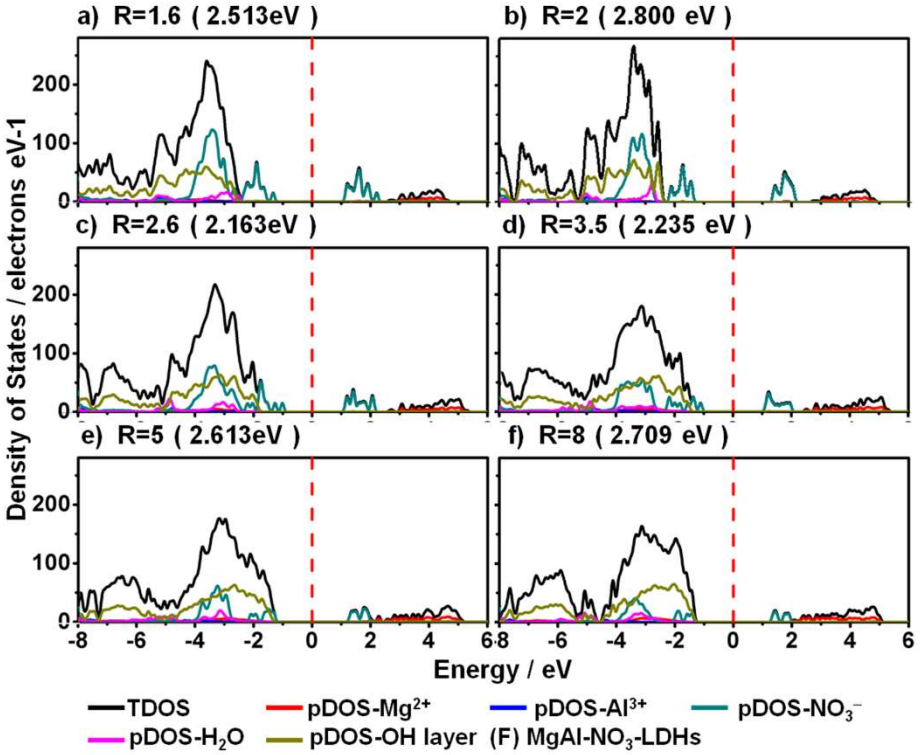
a) R=1.6 (2.513eV)
b) R=2 (2.800 eV)
c) R=2.6 (2.163eV)
d) R=3.5 (2.235 eV)
e) R=5 (2.613eV)
f) R=8 (2.709 eV)
Density of States / electrons eV-1
Energy / eV
TDOS
pDOS-Mg2+
pDOS-Al3+
pDOS-NO3−
pDOS-H2O
pDOS-OH layer
(F) MgAl-NO3-LDHs

39

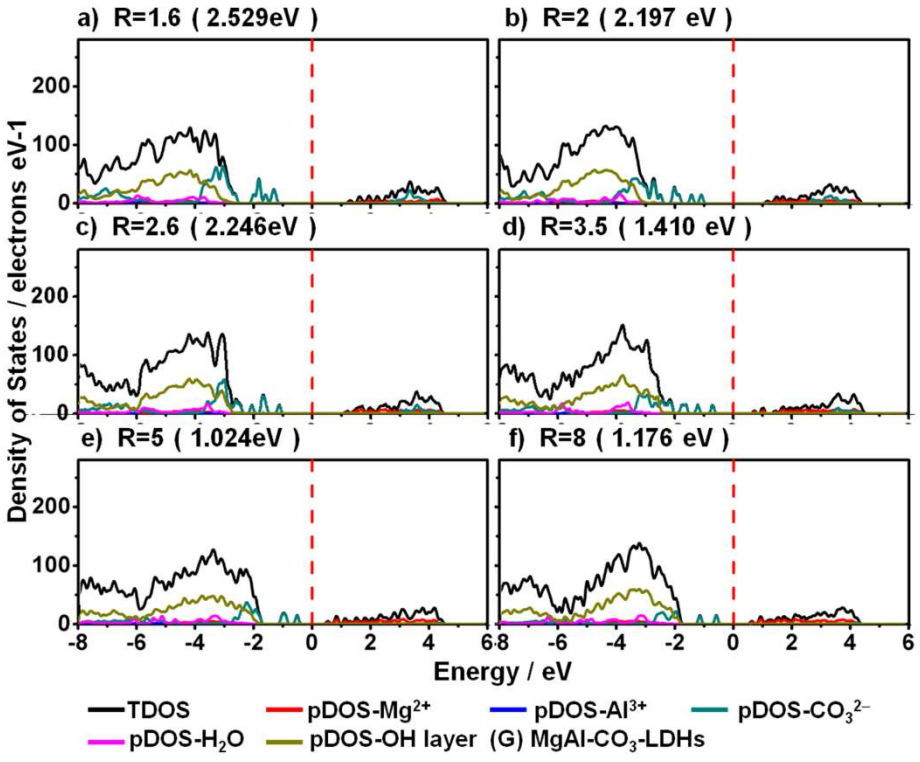
a) R=1.6 (2.529eV)
b) R=2 (2.197 eV)
c) R=2.6 (2.246eV)
d) R=3.5 (1.410 eV)
e) R=5 (1.024eV)
f) R=8 (1.176 eV)
Density of States / electrons eV-1
Energy / eV
TDOS
pDOS-Mg2+
pDOS-Al3+
pDOS-CO32–
pDOS-H2O
pDOS-OH layer
(G) MgAl-CO3-LDHs

40

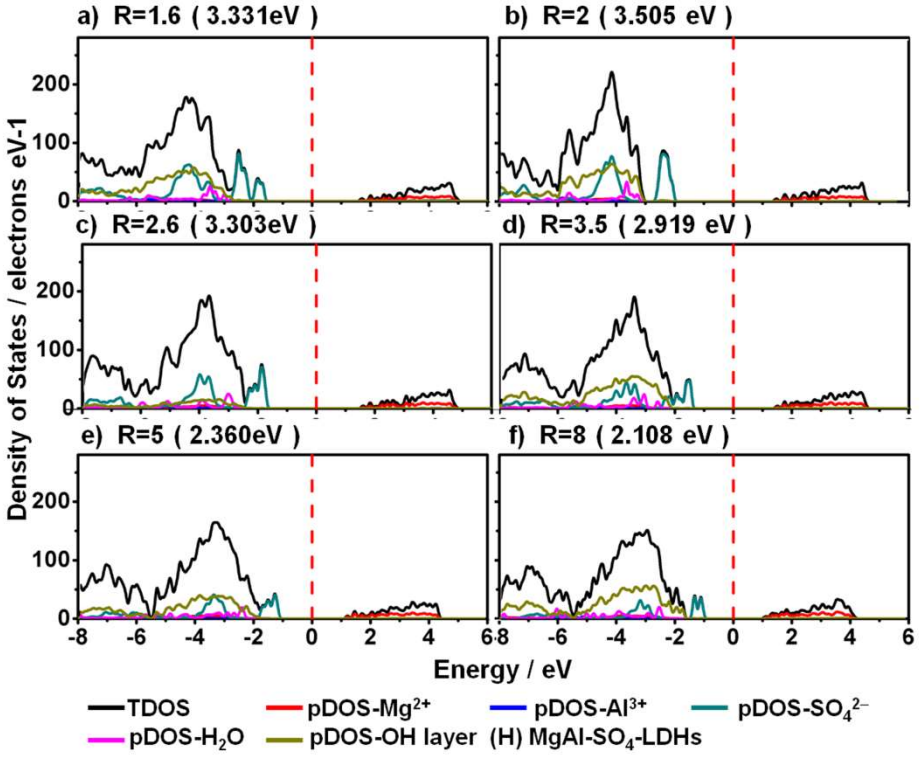
a) R=1.6 (3.331eV)
b) R=2 (3.505 eV)
c) R=2.6 (3.303eV)
d) R=3.5 (2.919 eV)
e) R=5 (2.360eV)
f) R=8 (2.108 eV)
Density of States / electrons eV-1
Energy / eV
TDOS
pDOS-Mg2+
pDOS-Al3+
pDOS-SO42–
pDOS-H2O
pDOS-OH layer
(H) MgAl-SO4-LDHs

41

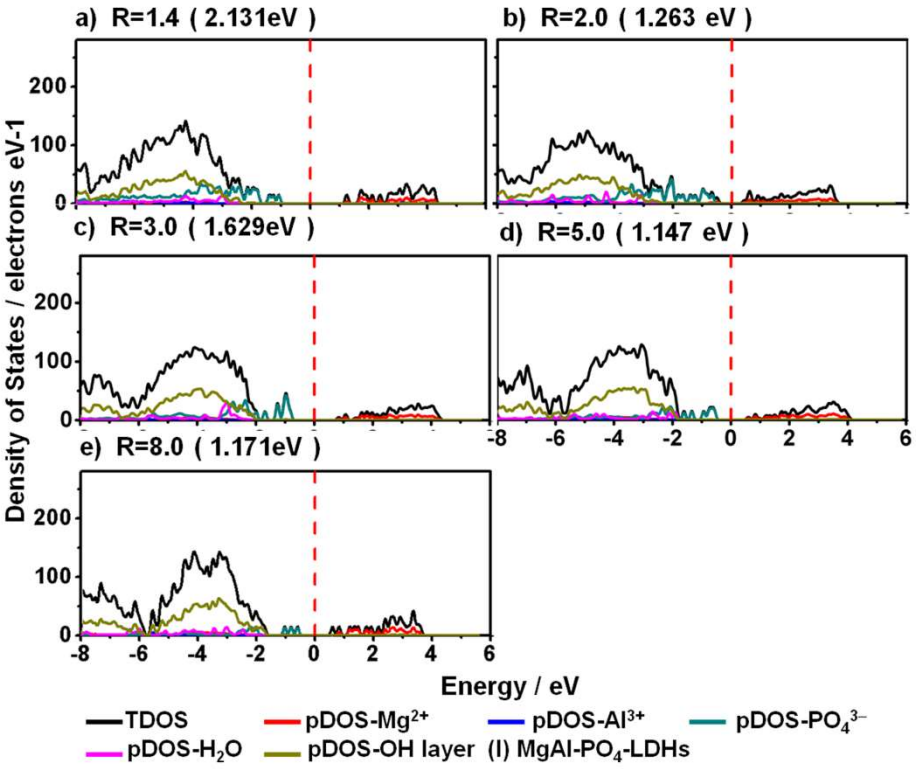

Fig. S9. Total density of states (TDOS) and partial density of states (PDOS) for the MgAl-A-LDHs intercalated with different interlayer anions (A= F^-, Cl^-, Br^-, I^-, OH^-, NO_3^-, CO_3^{2-}, SO_4^{2-}, PO_4^{3-}) and different *R* (Mg^{2+}/Al^{3+}). The Fermi energy is shown as a dashed vertical line, and has been set as 0 eV.

References

S1 L. Yan, S. Hu, J. M. Duan and C. Y. Jing, *J. Phys. Chem. A,* 2014, **118**, 4759–4765.

S2 Y. M. Fan, Y. Q. Zhao, Z. W. Zhu, W. Du and L. L. Li, *J. Phys. Chem. A,* 2017, **121**, 7385–7329.

S3 A. Arnold, V. Terskikh and Q. Y. Li, *J. Phys. Chem. C,* 2013, **117**, 25733–25741.

S4 H. Yan, M. Wei, J. Ma, D. G. Evans and X. Duan, *J. Phys. Chem. A,* 2010, **114**, 7369–7376.

55 S5 S. Aisawa, S. Takahashi, W. Ogasawara, Y. Umatsu and E. Naruta, *J. Solid State*

56 *Chem.,* 2001, **162**, 52–62.

57 S6 A. Dias, L. Cunha and A. C. Vieira, *Mater. Res. Bull.,* 2011, **46**, 1346–1351.

58 S7 F. Cavani, F. Trifrio and A. Vaccari, *Catal. Today,* 1991, **11**, 173–301.

59 S8 S. Ishihara, P. Sahoo, K. Deguchi, S. Ohki, M. Tansho, T. Shimizu, J. Labuta, J. P. Hill, K. Ariga, K. Watanabe, Y. Yamauchi, S. Suehara and N. Iyi, J. Am. Chem. Soc., 2013, 135, 18040–18043.